Journal of South American Earth Sciences 115 (2022) 103764

Contents lists available at ScienceDirect

Journal of South American Earth Sciences

journal homepage: www.elsevier.com/locate/jsames

Influence of structures and lithologies in the morphology and localization of Au–Ag mineralization at Martinetas deposit, Don Nicolas mine, Deseado Massif, Argentina

Facundo.J. De Martino [a,b,e,*], Sebastián M. Jovic [c,d,e], Luciano López [a,b,e], Horacio J. Echeveste [a,e]

[a] Instituto de Recursos Minerales, Facultad de Ciencias Naturales y Museo, Universidad Nacional de La Plata, Calle 64 y Calle 120, La Plata, Buenos Aires, Argentina
[b] Consejo Nacional de Investigaciones Científicas y Técnicas, Godoy Cruz, 2290, Buenos Aires, Argentina
[c] Cerrado Gold Inc., Minera Don Nicolas, Ruta 3, km. 2085,5, Estancia El Cóndor, Paraje Tres Cerros, Santa Cruz, Argentina
[d] Universidad de Buenos Aires, Facultad de Ciencias Exactas y Naturales, Departamento de Ciencias Geológicas, Pabellón II, Ciudad Universitaria, Intendente Guiraldes, 2160, Núñez, Buenos Aires, Argentina
[e] Facultad de Ciencias Naturales y Museo, Universidad Nacional de La Plata, Calle 64 y Calle 120, La Plata, Buenos Aires, Argentina

ARTICLE INFO

Keywords:
Structural control
Lithological control
Epithermal
Low sulfidation
Gold-silver deseado massif

ABSTRACT

This work describes the structural and lithological controls that affect the distribution, orientation, and precipitation mechanism of mineralization in the Martinetas district, from the structural context and the analysis of the role played by the geological units that host the mineralization. Martinetas is a low sulfidation epithermal gold and silver mining district located in the northeastern sector of the Deseado Massif, Argentina. The district is characterized by numerous quartz veins, sheeted veinlets and breccias, developed in pyroclastic and volcanic rocks of the Bahia Laura Volcanic Complex.

The analysis of fractures, faults and host rocks of the vein systems show that the main factors controlling the formation and distribution of the mineralization are the lithology, deformation style and fault kinematics. Their interplay led to positive feedback between the evolution of plane aperture through time, strain localization and the resulting mineralization. Vein orientations are indicative of a NE-SW extensional stress field at the time of hydrothermal fluid ascend, which favored fluid input and pervasive flow within the active fractures and the matrix of the geological units. Subsequently, cyclic channelized fluid flow during repeated fluid input caused extensive veining and numerous filling events. A link between hydrothermal organic matter and the presence of gold in the vein system has been recorded.

Knowledge of the structural and lithological controls that set the structure and the distribution of higher grades ore shoots of the mineralization in the Martinetas district constitutes information of high value as an exploratory tool for the region.

1. Introduction

The transport of fluids from metals sources to the sites where the ore is deposited responds to pressure gradients of these fluids, buoyancy effects and the permeability of the host rock (Cox et al., 2001). High permeability and high-pressure gradients lead to high flow gradient, resulting in significant heat, fluid, and metal transport, favorable for the formation of epithermal deposits (Ingebritsen and Appold, 2012). Magmatic-hydrothermal fluids heated at depth, commonly due to the emplacement and crystallization of magmas, ascend to the depositional sectors in the form of plumes due to their low density, following high permeability planes, generally represented by faults.

The three-dimensional distribution of faults and fractures is primarily controlled by fluid gradient and stress field but may also be influenced by pre-existing mechanical anisotropies and rheological characteristics of the host rocks (Cox et al., 2001). Faults act as channels for fluid movement and portions with greater openness may increase hydrothermal fluid flow and thus promote the development of ore shoots registered in many low sulfidation epithermal systems (Corbett, 2002). The zones of greatest dilatancy are often related to changes in the

* Corresponding author. Universidad Nacional de La Plata, Calle 64 y Calle 120, La Plata, Buenos Aires, Argentina.
E-mail addresses: facundodemartino@gmail.com, facundodemartino@fcnym.unlp.edu.ar (Facundo.J. De Martino).

https://doi.org/10.1016/j.jsames.2022.103764
Received 28 June 2021; Received in revised form 16 February 2022; Accepted 8 March 2022
Available online 11 March 2022

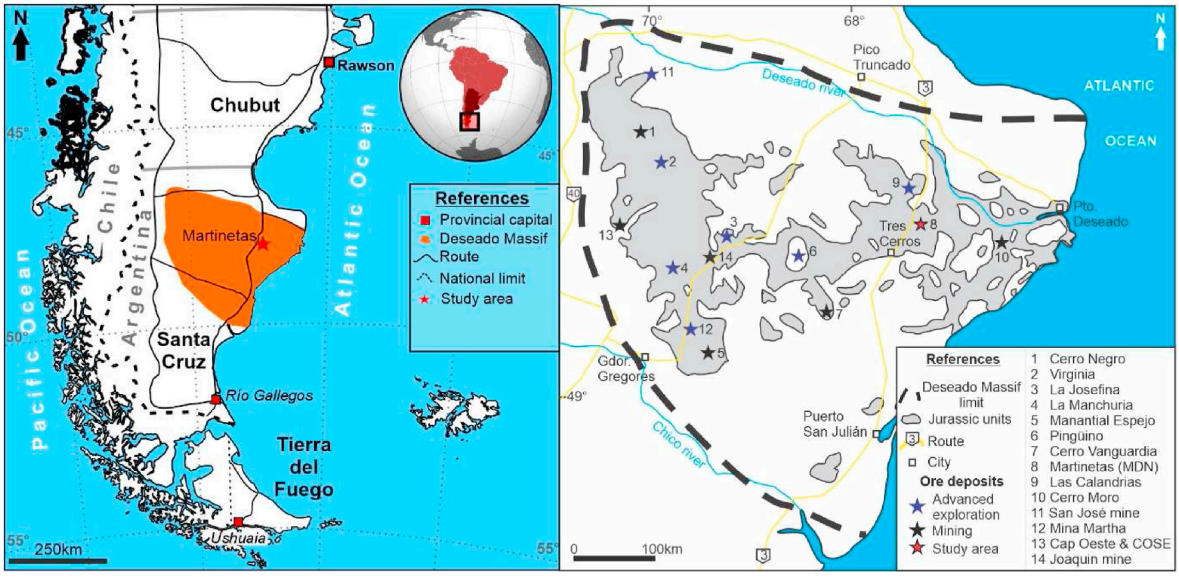

Fig. 1. Location of the study area and main Au–Ag deposits and prospects in the Deseado Massif epithermal province, Argentinian Patagonia. Modified from Schalamuk et al. (1999), updated data from Secretaría de política minera (2020).

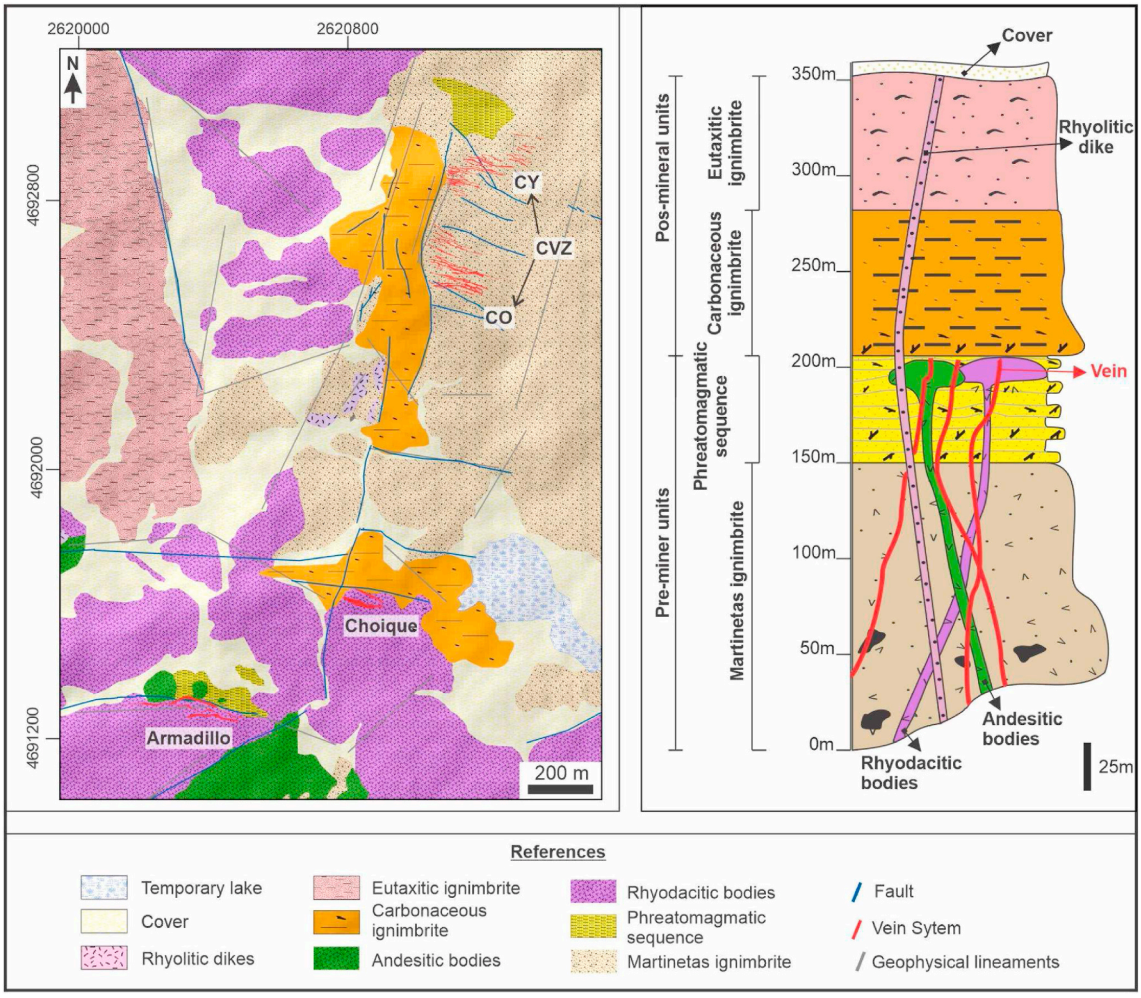

Fig. 2. Map and geological profile of the Martinetas district and demarcation of operating sectors. *CVZ: Central Vein Zone; CY: Coyote; CO: Cerro Oro.

strike of the hosting faults. Also, the termination of fault zones, fault relays, and jogs, bifurcations and branch lines are sectors of high fracturing. Permeability increases in favorable structural zones, developing areas with high potential for ore deposition (Cox et al., 2001; Micklethwaite, 2009; Faulds et al., 2011; Rowland and Simmons, 2012; Rhys et al., 2020).

In volcanic sequences, epithermal veins may be confined only to competent rocks, while the less competent ones host only barren fault structures (Corbett, 2007) or thin and discontinuous fractures/faults.

Chemically reactive host rocks can generate the precipitation of solutes transported by the hydrothermal fluids, promoting their deposition. The spatial association of gold mineralization with carbonaceous rocks is a notable feature in gold-rich systems (Cline et al., 2005; Large et al., 2011; Fuchs et al., 2017). Organic matter and its derivatives can have different active roles to form or preserve metalliferous deposits, e.g. concentration and reduction of metals (Leventhal and Giordano, 1997).

Martinetas is an active mining district located in the northeastern sector of the Deseado Massif, 220 km from Puerto Deseado city (Fig. 1). The deposit is currently mined for gold and silver by Cerrado Gold Inc., producing from three discrete vein systems (Fig. 2): Armadillo, Choique and Central Vein Zone, which have characteristics of a low sulfidation epithermal veins composed of numerous fault-fill quartz veins, sheeted extensional veinlets and vein breccia (De Martino et al., 2020b). The Central Vein Zone (CVZ), is represented by a sheeted vein system with some veins greater than 2 m. In Armadillo the mineralization is characterized by veins up to 7 m thick with veinlets and breccias associated. Choique sectors present thicker veins (exceeding 5 m thick in some sections) with breccias and associated stockwork.

The Martinetas district is part of the Don Nicolas mining project, recently acquired by Cerrado Gold mining company. It has been in operation since 2016. It has a total measured and indicated resources of 1.14 Mt @ 4 g/t Au and 10.41 g/t Ag (Technical Report, 2018) at a cut-off grade of 1.6 g/t. The tonnage and grade are slightly below the limit that encompasses the category of sub-economic deposits (Hedenquist et al., 2000), so the Don Nicolás mining project complements its exploitation with that of the La Paloma district, located 40 km to the NW. Beyond the low tonnage, the martinetas deposit is one of the few deposits in exploitation in the eastern sector of the Macizo del Desierto.

This work describes the structural and lithological controls that affect the distribution, orientation, and precipitation process in the Martinetas deposit, from the structural context of the Deseado Massif and the district. It also analyses the physicochemical role played by the geological units affected by the hydrothermal system. Knowledge of the structural and lithological controls that condition the structure and the distribution of higher grades ore shoots of the mineralization in the Martinetas district constitutes information of high value as an exploratory tool for the region.

2. Methodology

This study is based primarily on mine mapping, and more than 1500 m of diamond drill cores logging corresponding to vein intercepts and host rocks. The samples were analyzed in detail from the mineralogical and textural characterization of the mineralizing pulses, in hand samples and polished and thin sections under an Olympus model BX53 microscope equipped with an Olympus model UC30 digital camera. The organic matter was determined from Raman spectrometry on a Jasco microscope model NRS-4100 and kerogens were determined under microscope with reflected light and oil immersion on a CRAIC 508 PV™ Microscope Spectrometer. Both analyses were carried out at the microscopy and Raman spectroscopy laboratory of YPF Tecnología (YTEC). The determination of the mineral species and chemical composition was performed at the Laboratory of Electron Microscopy and X-ray Analysis (LAMARX), of the Universidad Nacional de Córdoba, by means of a scanning electron microscopy (SEM) analysis, executed by means of a FE-SEM Σigma mineral microscope. The X-ray analyses were carried out in a Philips X'Pert PRO diffractometer model 2009 with Cu anode, in the Centro de Investigaciones Geológicas (CIG; UNLP-CONICET).

The structures, ore shoots and geological bodies were modeled using LeapfrogGeo by triangulation (interpolation) between geological sections (explicit model; Cowan et al., 2003) combined with mathematical function from drill holes data (implicit model; Vollgger et al., 2015).

3. Deseado massif

3.1. Regional geology

The Deseado Massif is one of the main morphostructural regions of southern Patagonia (Fig. 1), covering a surface of about 60,000 km^2. The geology of the northeastern sector of the Deseado Massif is represented by a basement of metamorphic and igneous rocks assigned to the Río Deseado Complex, of probable Precambrian to Devonian age (Viera and Pezzuchi, 1976; Guido, 2004).

The development of a set of rift basins, product of the collapse of the Gondwanic orogeny (Haller, 2002; Ramos, 2008), resulted in the deposition of a thicker sequence of continental sediments of Permian age, gathered under the Tres Cerros Group (Herbst, 1965), which includes the La Golondrina Formation (Archangelsky, 1958) and La Juanita Formation (Arrondo, 1972). These are coarse-grained rocks (sandstones and conglomerates) with abundant fossil content.

Towards the Triassic, Pangea would have undergone a counterclockwise rotation (Riel et al., 2018) giving rise to a transtensional regime associated with an oblique subduction environment (Zerfass et al., 2004). This second extensional stage allowed the deposition of the sedimentary and volcanic sequence of the El Tranquilo Group (Haller, 2002). During the Upper Triassic to Lower Jurassic, a calc-alkaline magmatic belt of NNW-SSE distribution is implanted that crosses from the southwestern region of Río Negro province to northeastern Santa Cruz province (Navarrete et al., 2019), whose intrusive bodies are grouped under the name of Central Patagonian Batholith (Rapela et al., 1991). These rocks are represented in the Deseado Massif by the La Leona Formation (Arrondo, 1972), integrated by granites, tonalites and leucogranites (Rapela and Pankhurst, 1996), which origin would be linked to arc magmatism (Godeas, 1992; Rapela and Pankhurst, 1996) in an extensional-transtensional regime (Rapela et al., 1991; Rapela and Pankhurst, 1992) associated a low-angle, flat slab-type subduction (Navarrete et al., 2019).

Subsequently, and during most of the Jurassic, the southwestern region of Gondwana underwent a voluminous magmatic event dominated by an extensional tectonic regime, resulting in three volcanic events (Pankhurst et al., 2000) denominated V1 (188-178Ma), limited to the North Patagonian Massif and south of the Antarctic Peninsula, V2 (173-160Ma), located in the central and eastern sector of Patagonia and north of the Antarctic Peninsula, and V3 (157-145Ma) located west of Patagonia and north of the Antarctic Peninsula. The origin of magmatism has been historically related to the generation of three large Igneous Provinces (LIPs), known as Karoo, Ferrar and Chon Aike (Storey et al., 1992, 2013; Storey and Kyle, 1997). The latter covers much of Argentine Patagonia and the Antarctic Peninsula (Kay et al., 1989; Pankhurst et al., 1998), and is responsible for extensive bimodal volcanism (Féraud et al., 1999), represented in the Deseado Massif by the Bahía Laura Volcanic Complex (Pankhurst et al., 1993). Thus, these rocks would be related to an intraplate environment, associated with lithospheric extension (e.g., Riley et al., 2001; Márquez et al., 2011), product of the presence of a mantle plume (Storey and Kyle, 1997; Riley et al., 2001; Storey et al., 2013; Tassara et al., 2017).

Jurassic units make up more than 60% of the outcrops in this region of Patagonia (Fig. 1), and among them pyroclastic flows and fall deposits predominate, with a minority presence of lavas and sectors with a large number of dikes and domes (Guido, 2004).

The extension, magmatism and high thermal gradient were

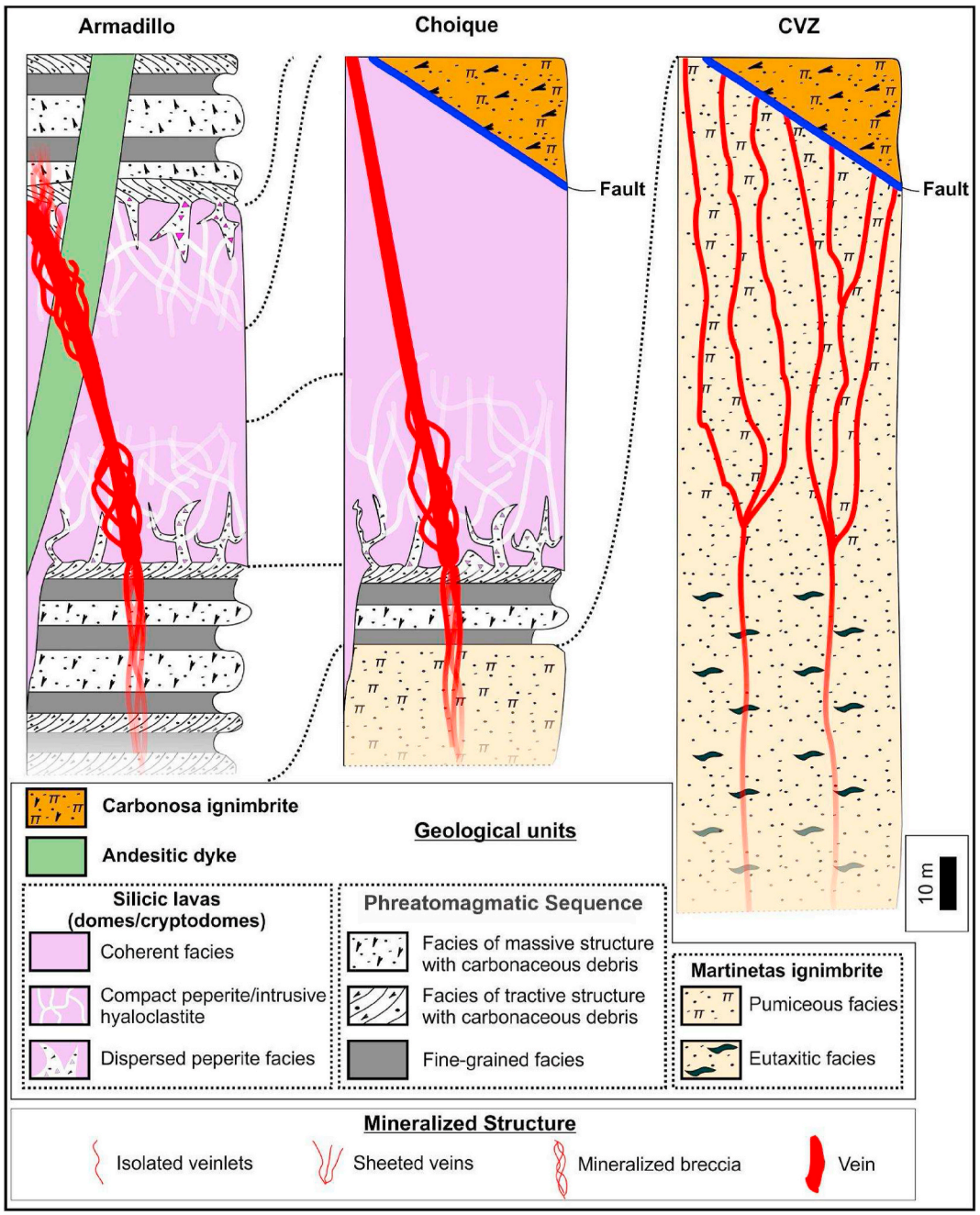

Fig. 3. Stratigraphic correlation between the Armadillo, Choique and Central Vein Zone (CVZ) sectors, showing the facies that compose the different units and the mineral structures developed in them.

responsible for the volcanic activity of the Bahía Laura Volcanic Complex and the installation of the hydrothermal systems of the Deseado Massif, evidenced by numerous hydrothermal paleosurfaces (Guido and Campbell, 2011) and metalliferous occurrences, mainly classified as low sulfidation epithermal (Schalamuk et al., 1999).

After the Jurassic volcanic event, we recognize sandstone outcrops assigned to the Baqueró and Laguna Palacios Formations (Hechem and y Homovc, 1987), of Lower Cretaceous age, and those corresponding to the continental sediments with pyroclastic participation of the Río Chico Formation (Simpson, 1933), Koluel Kaike Formation (Feruglio, 1949) and Sarmiento Formation (Feruglio, 1949), corresponding to the Tertiary, on which the marine strata of the Patagonian (Zambrano and Urien, 1970) and continental deposits of the upper Tertiary of the Santa Cruz Formation (Ameghino, 1898) are supported.

The Cenozoic is highlighted by extensive basaltic plateau, represented in the eastern sector of the Deseado Massif by the La Angelita Basalt (Panza, 1982), produced from the southwest to northeast migration of an asthenospheric window, generated by the subduction of the triple point between the South American, Pacific and Nazca plates (Ramos and Kay, 1992).

3.2. Structural framework

The Deseado Massif records a complex deformation history, given the variations that its geotectonic setting has undergone since the Paleozoic.

The basement of the Deseado Massif shows a dominant structural trend with a direction N35°W (Giacosa et al., 2002). According to

Fig. 4. Photographs of the open pits **(a)** Cerro Oro (CVZ) and **(b)** Armadillo, showing the structure of the vein/vein system.

Fracchia and Giacosa (2006) the basement in the northeast of the Deseado Massif shows evidence of transcurrent deformation of dextral NNW structures and ductile-brittle strain, corresponding to the Late Silurian-Devonian, representing an important regional shortening in NNE-SSW to NE-SW direction and suggesting that the geodynamic context of the Paleozoic orogen of the Deseado region in this sector has been maintained during the Late Silurian-Early Permian period.

The Jurassic of the Deseado Massif is characterized by rifting. It has been part of the initial division of Pangea, with the breakup of the Weddell Sea triple junction around 177 to 168 Ma and originated the development of rift basins with grabens and hemi-grabens filled by syn-depositional volcanic and volcaniclastic products of Bahía Laura Volcanic Complex (Homovc and Constantini, 2001).

Continued extension, magmatism and the formation of associated hydrothermal systems gave rise to the development of low to intermediate sulfidation epithermal veins which have predominant NW strike (Echeveste, 2010). The distribution and orientation of these coincide with regional geological lineaments of NW and NNW orientation (Guido and Campbell, 2011; Giacosa et al., 2010), which imply reactivation of Lower Paleozoic NNW to NW basement structures (Homovc and Constantini, 2001; Giacosa, 2020). In turn, the effusive facies are associated with ENE and NNW lineaments, showing that the volcanic materials were mostly extruded through the Jurassic extensional fractures, occasionally generating caldera structures (Guido, 2004).

Post-mineral deformation coincided with the return to ENE-normal extension that may have signaled a return to regional stress dictated by subduction to the west (roll-back of the subducted slab: Navarrete et al., 2019).

Multi-scale structural analysis of Au–Ag mineralization in veins shows that the distribution of the districts is regionally controlled by normal to oblique slip fault system, in response to the NE-SW extensional direction (Jovic et al., 2014; Fernández et al., 2019). However, each district shows local controls dependent on its own geological, lithological and structural characteristics (Jovic et al., 2014).

4. Local geology

4.1. Hosting volcanic sequence

The Martinetas deposit is hosted by the Jurassic Bahía Laura Volcanic Complex (BLVC; De Martino et al., 2020a). The BLVC is locally represented by extensive pyroclastic (dilute and dense) and interbedded coherent silicic and meso-silicic volcanic units. This sequence is covered by massive ignimbrites and intruded by a swarm of rhyolitic dykes (Fig. 2).

The oldest volcanic unit in the Martinetas District is the Martinetas Ignimbrite, which outcrops in the northeastern sector of the district (Fig. 2). It is a poorly-sorted, massive crystal-rich rhyolitic ash-flow tuff, with a thickness of at least 200 m. Its base has not been intercepted by drillings.

After a volcanic hiatus, deposition of sediments with associated plant fossils occurred. The sequence and underlying tuff were subsequently intruded by subvolcanic bodies of rhyodacitic composition and are associated with phreatomagmatic breccia and tuff of what is termed Phreatomagmatic Sequence. It is composed of an alternating centimeter to meter-thick layers of massive ash-flow tuffs and surge deposits with wavy bedding, cross-stratified and planar laminations and the presence of small fragments of carbonized wood. This unit has a poor surface expression, is better developed in the Armadillo area and the Central Vein Zone (Fig. 2), and its thickness is at least 120 m. The phreatomagmatic origin of this unit was interpreted by De Martino et al. (2017) based on its thickness, the presence of accretionary lapilli, syn-sedimentary deformation structures and bomb impact structures. The interaction of magma with unconsolidated sediments (Phreatomagmatic Sequence) and the water table produce peperite and hyaloclastite breccia at the edges of the subvolcanic intrusions (De Martino et al., 2020a). The generation of these facies is only feasible in a shallow environment, less than 1600 m deep (Kokelaar, 1982).

Following the previous units, an effusive volcanic cycle represented by rhyodacitic extrusive and subvolcanic bodies occurred in the southwestern portion of the district. This is represented by domes, cryptodomes, lava flows and several dykes, which were informally named the Rhyodacitic Lava unit (Fig. 2). These in turn are intruded by a set of porphyritic dykes of andesitic composition (Andesitic Lavas in Fig. 2), assimilating blocks of the Phreatomagmatic Sequence in its ascent.

After the intrusion of the rhyodacite and andesite units, a period of intense hydrothermal activity occurred in the district overprinting these and underlying units and giving rise to the Martinetas Au–Ag epithermal deposit that is currently being mined (De Martino, 2021).

Subsequently, another explosive volcanic cycle developed, which originated the Carbonaceous ignimbrite, a poorly-sorted rhyolitic ash flow tuff. Its outcrops are espacially associated with those of the Phreatomagmatic Sequence and are better developed toward the north of the Choique Area and west of the Central Vein Zone (Fig. 2). This unit is also characterized by the presence of carbonized wood fragments.

The Eutaxitic Ignimbrite overlies the previous units to the northwest

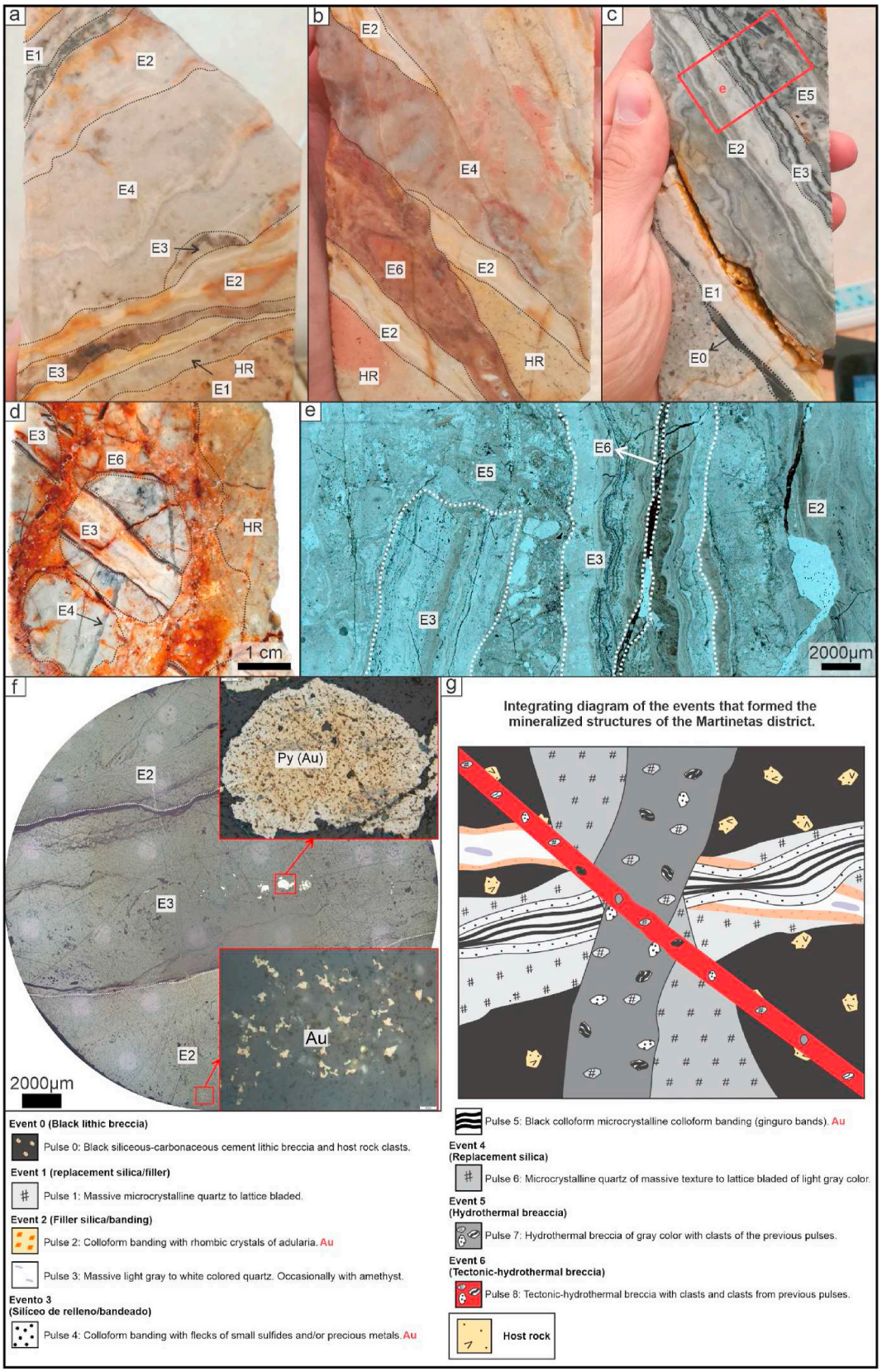

Fig. 5. Paragenesis of mineralizing events in the Martinetas district. **(a**,**b**,**c** and **d)** HQ Core drillhole photographs (diameter: 63,5 mm) showing the temporal relationships between the different events forming the fault hosting veins in the Martinetas district. The red rectangle in figure c shows the location of the thin section corresponding to figure e. *HR: Host Rock. **(e)** Photomicrograph of thin sections showing pulse textures and opaque flecks present in event 3. **(f)** Photomicrograph of a polished specimen containing events 2 and 3 with gold (Au) and auriferous pyrite (Py), respectively. **(g)** Schematic diagram of the temporal relationship between the hydrothermal pulses that make up the mineralized structures of the Martinetas district vein system, discriminated in 6 events.

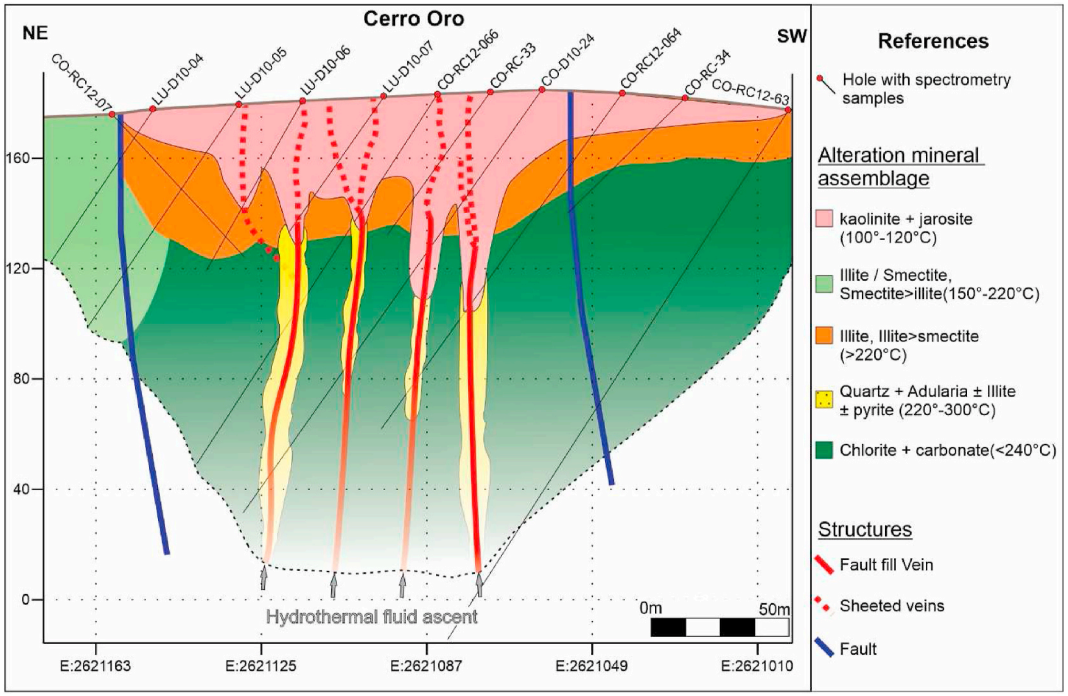

Fig. 6. Schematic diagram of alteration mineral assemblage in CVZ (Cerro Oro).

of the district (Fig. 2). This is a poorly-sorted matrix supported ash flow tuff of rhyolitic composition that is characterized by a moderate to high degree of welding and thicknesses exceeding 50 m.

Finally, a swarm of rhyolitic porphyritic dykes was emplaced, cutting the whole sequence from SW to NE. These dykes represent the last stages of volcanism in the district (Fig. 2). The absence of hydrothermal alteration and veins in the last three units allows us to characterize them as post-mineral in nature.

The south of the district is characterized by veins up to more than 5 m thick, hosted by the rhyodacitic and, to a lesser extent, andesitic bodies, forming the main host rocks of the Armadillo and Choique sectors (Fig. 3). Hydrothermal fluids interaction with the host rock (Phreatomagmatic Sequence) results in the generation of peperitic breccias and intrusive hyaloclastites (De Martino et al., 2020a), where mineralization occurs as lithic breccias with hydrothermal quartz cement, taking advantage of the primary texture for their injection (Fig. 3). Similarly, the Phreatomagmatic Sequence acts as host rock for the mineralization, with the same texture as the breccias at the edge of the subvolcanic bodies.

The northern Martinetas, represented by the Central Vein Zone, comprises only the Martinetas ignimbrite as host rock for mineralization. Although no marked discontinuities have been observed within this unit in the mapping and logging of drill cores, the gradual transition in the degree of deformation of the pumice between 70 and 100 masl in the Coyote and Cerro Oro sectors, respectively. This distinction in texture allowed differentiating two facies within the ignimbrite, a Eutaxitic facies at the base and a pumiceous facies above (Fig. 3). The gradual boundary between the two facies coincides with the densification of the veinlets towards the surface, quantified from the vein/drilled meter ratio (Fig. 3).

4.2. Mineralization

The district has two well differentiated sectors from the point of view of the bedrock and vein structure. To the north, the Central Vein Zone sector (CVZ) includes the Coyote open pit, located to the north and the Cerro Oro pit to the south. The vein system is composed of numerous sub-parallel centimeters veinlets and few veins up to 2 m thick which have NW and WNW trends, forming vein sets that cross the pits from ESE to WNW (Fig. 4a). Mineralization is mainly associated with scarce veins that do not exceed 2 m in thickness and a large development of thinner veins with a parallel distribution (sheeted vein; Fig. 4a) and to a lesser extent, stockwork.

On the other hand, to the south of the district, the Armadillo (Fig. 4b) and Choique sectors present thicker veins (exceeding 5 m in some sections) with breccias and associated stockwork. Both sectors were mined in open pits.

Before the development of quartz veins, a faulting episode is interpreted (Event 0; E0) to have occurred (De Martino, 2021) as a network of fractures.

The hydrothermal events commenced with Event 1 (E1), which comprises a pulse (P1) formed by a network of veinlets and small breccia veins of colorless to light gray quartz, of pre-mineral nature. Event 2 comprises two infill/replacement pulses of colloform banded texture, formed by bands of micro-to cryptocrystalline quartz-adularia (Pulse 2) with gold and electrum disseminated, followed by (Pulse 3) bands of quartz of saccharoidal texture with adularia of massive texture and light gray to white color. Event 3 corresponds to two filling pulses with colloform banded texture, one with very fine-grained pyrite, sphalerite, chalcopyrite, gold and electrum (ginguro bands; Pulse 4) with carbonaceous debris spatially associated to gold and the other with gray and black cryptocrystalline bands (Pulse 5) with scarcegold, pyrite and sphalerite disseminated. Event 4 is light gray to white microcrystalline quartz, generally with lattice quartz after calcite replacement texture. Event 5 comprises a microcrystalline quartz cement breccia (Pulse 7), generally dark gray in color, incorporating fragments of the previous vein stages and bedrock as lithic fragments. The final stage, event 6 corresponds to quartz cemented breccia consisting of silica with iron oxides and hydroxides (Pulse 8), showing a tectonic component (cataclasite).

The temporal relationship of the different events keep (Fig. 5a–e), allowed us to confirm events 2 and 3 as the ore containers at the sequence of events that formed the mineralized structures (Fig. 5f).

The textural and mineralogical characteristics found in the Martinetas district, comprising predominantly colloform and costriform quartz bands, rhombic adularia, pseudomorphic carbonate quartz

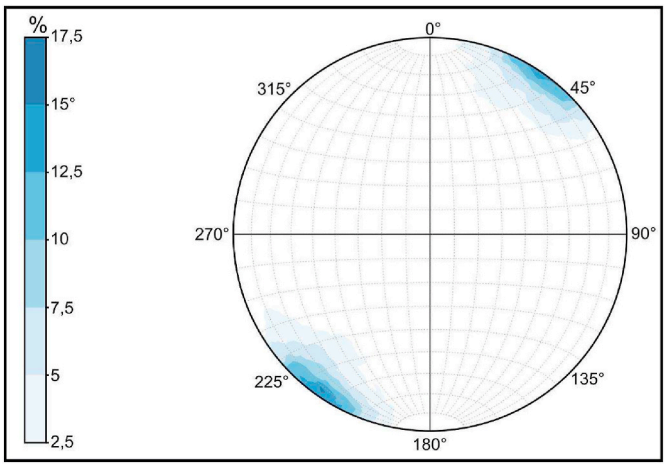

Fig. 7. Pole diagram showing vein/vein orientation in the Martinetas district based on the 768 measurements.

(lattice bladed) and ginguro bands, suggest boiling as the main process responsible for mineral deposition (Henley et al., 1984; Browne and Ellis, 1970; Tharalson et al., 2019).

4.3. Alteration

The hydrothermal alteration presents a superposition of synchronous and post-mineralization events.

Adjacent to the epithermal veins and veinlets, there is an aggregate of quartz-adularia and illite, covering the first few centimeters a few meters from the structures, followed by interstratified illite/smectite (Fig. 6). Below the oxidation level (70 m below the surface on average), the alteration adjacent to the vein/vein system is accompanied by pyrite disseminations and towards the distal portions (tens of centimeters to tens of meters from the veins/veins), the bedrock presents mafic crystals altered to chlorite and plagioclase mainly to carbonates, forming a propylitic alteration, which is linked to the epithermal event related to the mineralization of the district (syn-mineral).

The shallow portion of the vein/vein systems and host rocks are affected by a penetrative and intense alteration to high crystallinity kaolinite accompanied by jarosite (Fig. 6), which covers from the

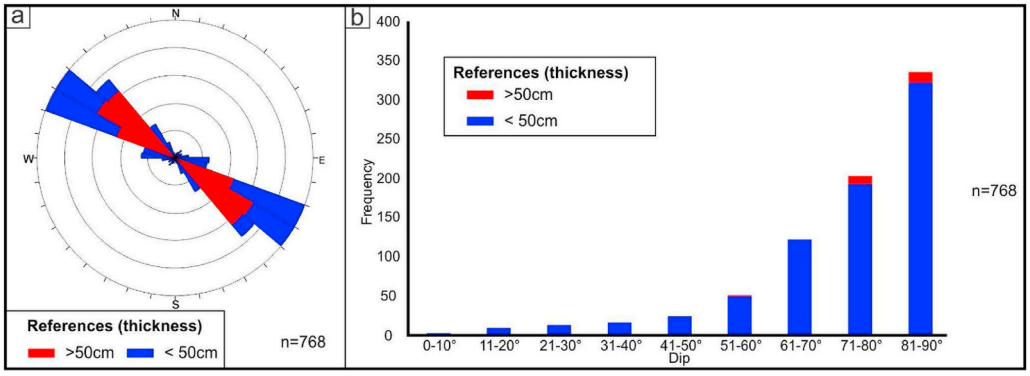

Fig. 8. Orientation of veins/veinlets in the Martinetas district. **(a)** Rose diagram indicating the frequency of orientation of veins/veinlets discriminated according to their thickness. Data correspond to a total of 768 measurements of vein/veinlets strike and inclination with Brunton compass within the open pits. **(e)** Frequency plot discriminating the dip of veins/veinlets according to their thickness.

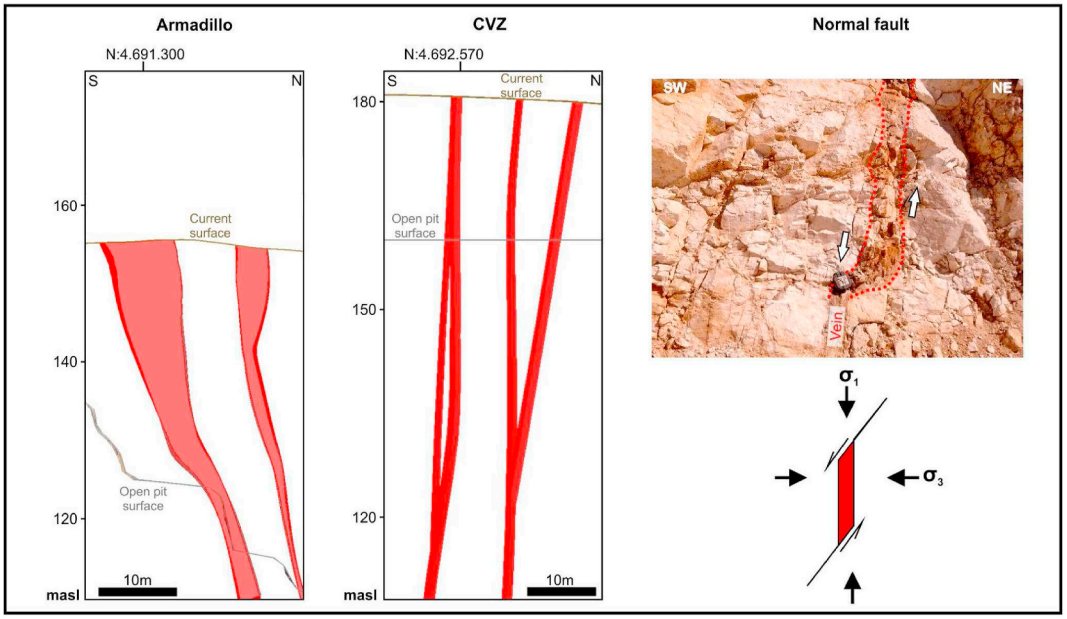

Fig. 9. Cross sections of the Armadillo veins and CVZ veinlets showing the structure at depth. The morphology of the fault allows the generation of dilational spaces or jogs from normal kinematics on the plane.

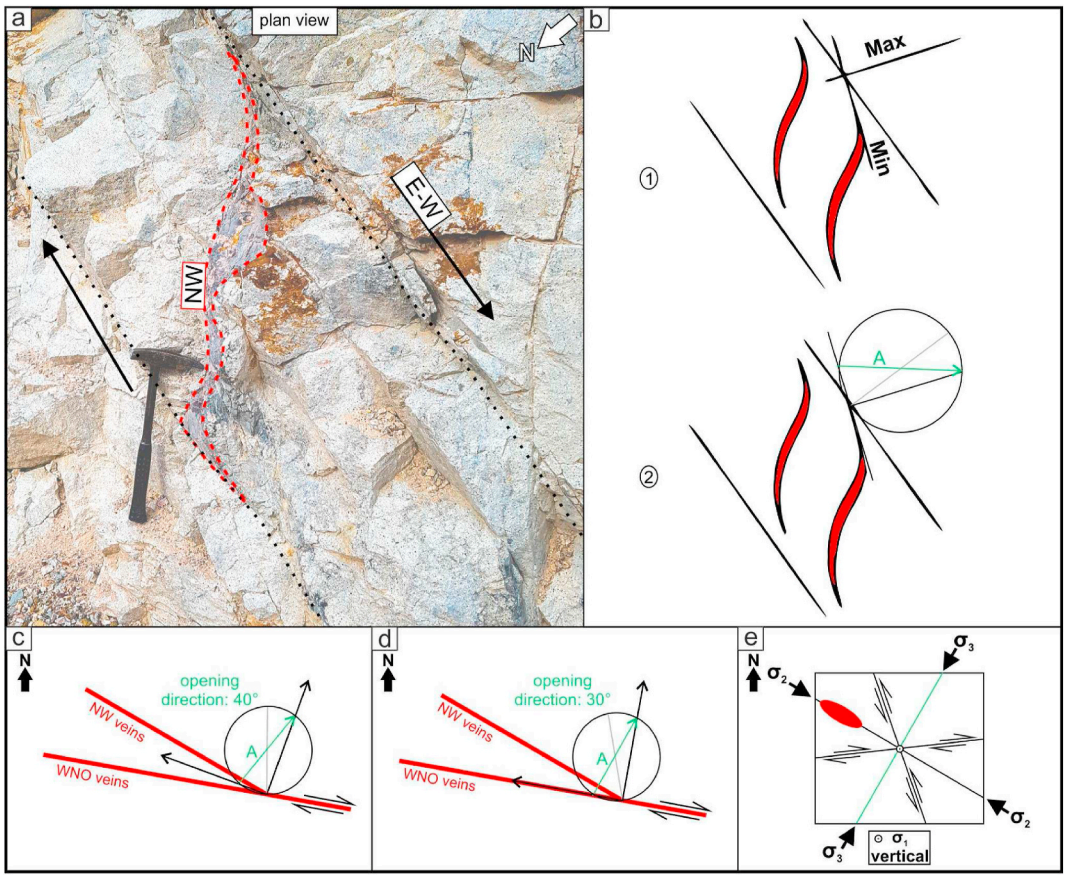

Fig. 10. **(a)** NW oriented sigmoidal veinlet in plan view, bounded by E-W planes, evidencing dextral shearing. **(b)** Schematic representation of the sigmoidal vein shear zone of Figure (a) with: (1) the identified orientations of the minimum and maximum principal axes of the deformation ellipse and (2) the displacement vector obtained according to the graphical resolution of McCoss (1986). **(c)** Graphical resolution according to the method of McCoss (1986) using the mean orientations of the NW and WNW veins under the assumption that both orientations have equal shear and aperture ratios. **(d)** Resolution plot according to McCoss (1986) method using the mean orientations of NW and WNW veins assuming that the WNW veins accommodate all shear deformation, while the NW veins accommodate all openness. **(e)** Theoretical stress diagram proposed for the study area compared with the orientation of the obtained opening vector.

topographic surface to some tens of meters in depth. The spatial association of subhorizontal silicifications, interpreted as silica cap and the association of kaolinite and jarosite allow interpreting this event as steam heated, formed from fluids charged with H2S that when interacting with O2 in the vadose zone forms H2SO4, generating sufficiently acidic conditions to form kaolinite (pH 2–3; Hedenquist and Arribas, 2019). The superposition of this alteration with that associated with the mineralization of the district evidences a relative ascent of the mineralized blocks with the consequent lowering of the water table in a late event of the epithermal system, post-mineral in nature.

This relationship allows us to interpret at least two alteration events. The first one corresponds to the ascent of hydrothermal fluids responsible for the Martinetas epithermal mineralization, formed by intermediate argillic alteration halos in the proximal zone and propylitic alteration distally to the veins/veins. The second is generated by the collapse of the system or the possible relative ascent of the mineralized blocks and consequent overprinting of a steam-heated environment over the vein/vein system and its associated alteration.

5. Structural control

5.1. Geometry and syn-mineral kinematics

As illustrated in Fig. 7, 768 vein orientation measurements from the Martinetas Mine workings illustrate that veins are predominantly subvertical and trend northwest.

Vein segments were classified according to thickness. A rose diagram allows to visualize the vein orientation frequency classified by thickness (Fig. 8a). The thicker veins (greater than 50 cm) have an azimuth range between 300° and 310°, while veins smaller than 50 cm have a more dispersed distribution.

The thickness of the structures also varies with respect to dip (Fig. 9b). Veins smaller than 50 cm show a large dispersion in dip, while structures thicker than 50 cm tend to have a subvertical dip (Fig. 8b).

The maximum opening of the veins is in subvertical directions, therefore σ1 is vertical and it is compatible with NE-SW extension at the time of mineralization (Fig. 9).

The maximum opening vector for the syn-mineral event can be determined either qualitatively or quantitatively. Qualitatively, the direction of maximum openness can be interpreted based on the observation of the morphology of the structure and the hydrothermal infill textures. In the veins of the district, the infill textures imply open space filling, such as the presence of crustiform/colloform banding (De Martino, 2021). In contrast, the WNW to E-W veins are thinner.

To further evaluate the kinematics implied by the veins, the graphical method of McCoss (1986) was used to determine the opening vector in mineralized structures. Being a simple geometrical construction, this graphical method has the advantage of being fast and expeditious. In the Martinetas district, field observations show that both vein systems are characterized by a mixed displacement with a shear component and an opening component. However, the shear component appears to be greater in the E-W structures than in the NW structures, where opening predominates over shear (Fig. 10a and b).

These characteristics allow us to pose two contrasting hypotheses

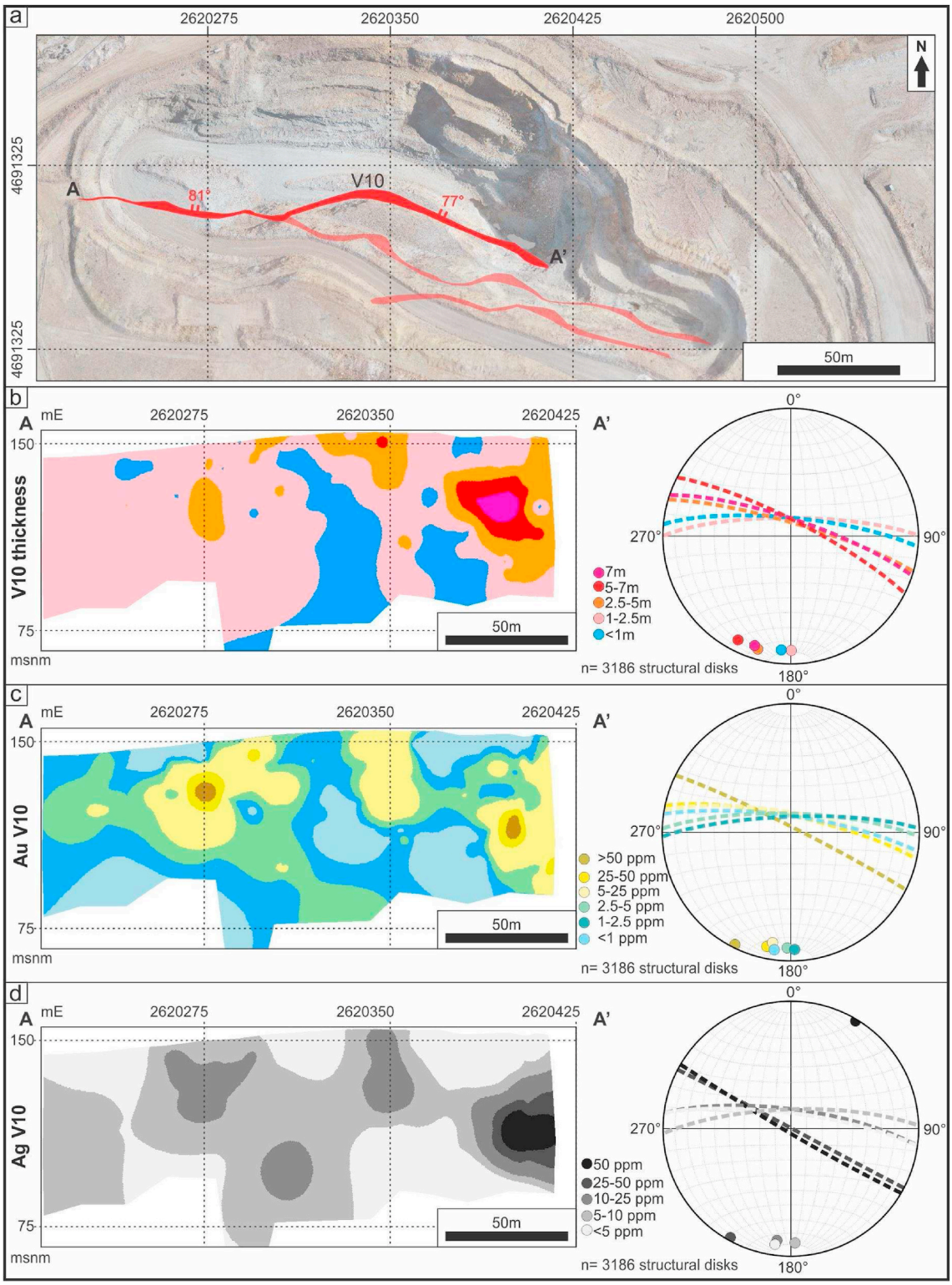

Fig. 11. **(a)** Location map of the V10 vein within the Armadillo pit. Longitudinal sections and stereograms of the V10 vein, showing the **(b)** thickness of the vein, **(c)** Au grade and **(d)** Ag grade and their relationship with the mean orientations of the vein that were derived from the 3D model and subdivided by Au and Ag grade. *The dotted lines of the stereograms indicate the mean attitude of the vein within each Au or Ag grade interval, and the great circles correspond to their poles. *The grades are Au or Ag per meter.

using the mean orientations of each vein system. The first assumes that both systems experienced equal proportions of shear and opening (Fig. 10c). The second hypothesis is that the E-W to WNW (290°) veins accommodate all shear deformation and that the NW (310°) veins represent a pure opening situation. According to the above and the geometric constructions (Fig. 10c and d), the opening direction would have an orientation between N30E° and N40E°, with an average value of N35E°, consistent with regional NE-SW extension at the time of mineralization (Fig. 10e).

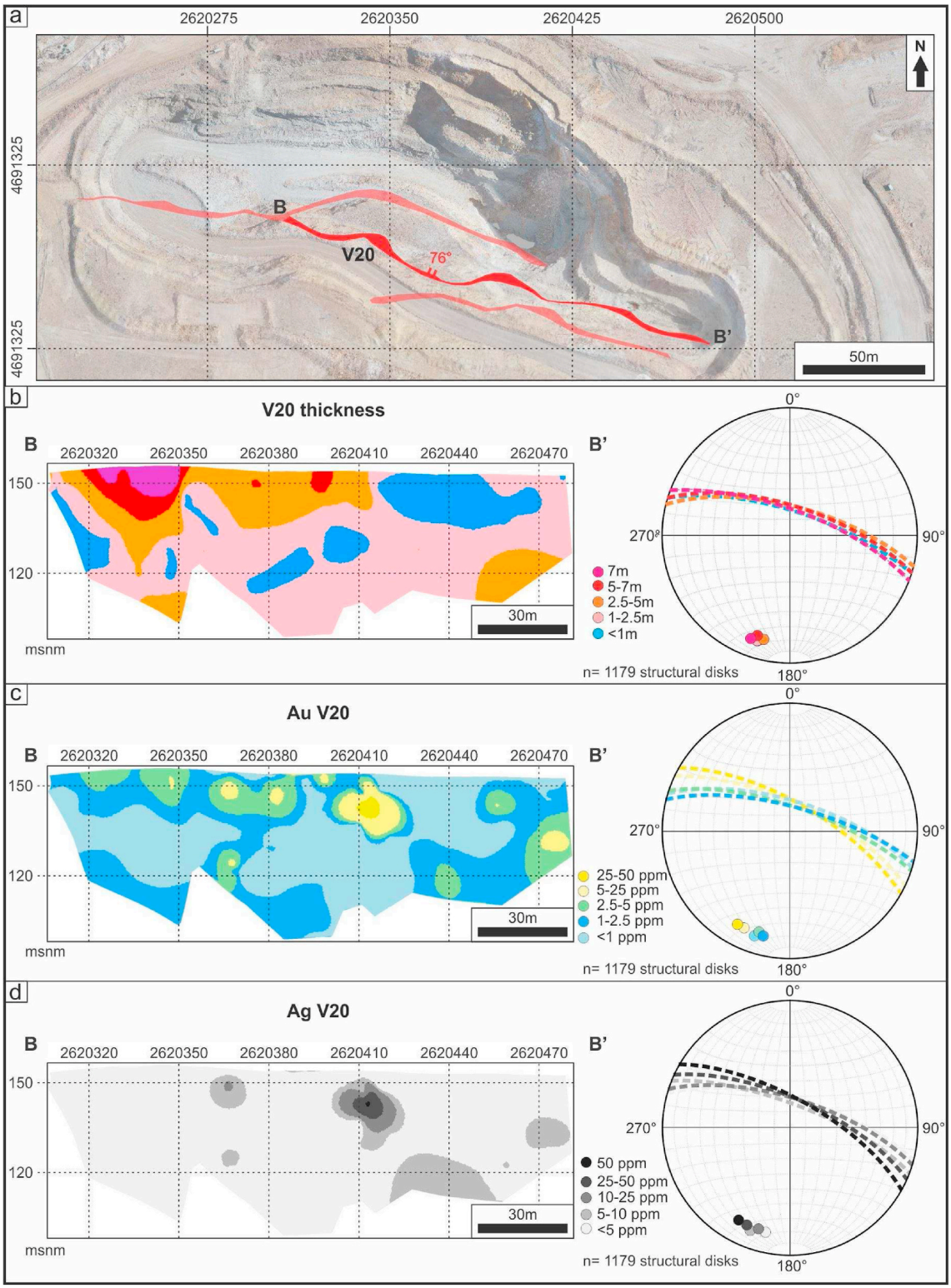

Fig. 12. **(a)** Location map of the V20 vein within the Armadillo pit. Longitudinal sections and stereograms of the V20 vein, showing the **(b)** thickness of the vein, **(c)** Au grade and **(d)** Ag grade and their relationship with the mean orientations of the vein that were derived from the 3D model and subdivided by Au and Ag grade. *The dotted lines of the stereograms indicate the mean attitude of the vein within each Au and Ag grade interval and the great circles correspond to their poles. *The grades are Au or Ag per meter.

5.2. 3D vein analysis: Armadillo

In the southern sector of the district, the Armadillo and Choique pits are currently being mined, allowing collection of a significant quantity of data and detailed structural analysis.

The mineralization in this sector consists of three main WNW trending veins of which have small variations in their azimuth and dip. The North vein, named V10 (Fig. 11) and the central vein, named V20 (Fig. 12), were analyzed.

Vein V11 (Fig. 11a), has a thickness greater than 5 m in its central

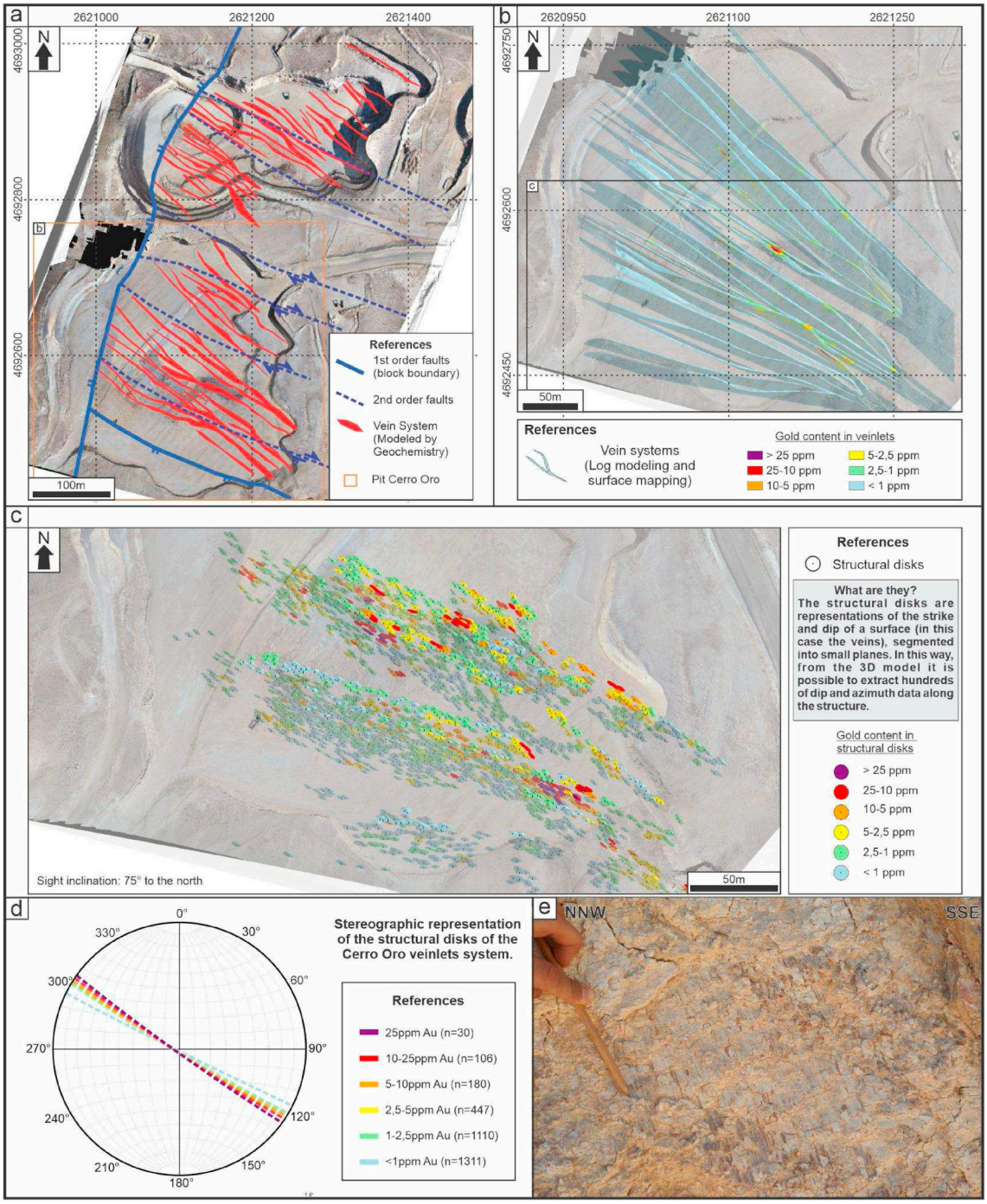

Fig. 13. **(a)** Map of the vein system modeled from gold geochemistry and major faults within the Cerro Oro (south) and Coyote (north) pits. **(b)** Map of the Cerro Oro veinlet system generated from interpolation of drill hole logging and surface mapping of the Cerro Oro pit, colored according to gold content within the veinlets. **(c)** Representation of the vein system by structural disks, classified according to the gold content in the structures. **(d)** Average stereographic projection of the structural disks representing the mineralized structures of Cerro Oro, differentiated by gold content. **(e)** Slickensides on the vein surface evidencing oblique normal setting.

and eastern sectors where it has a strike of 290–300° azimuth (Fig. 11b), showing a gradual decrease in its thickness in the E-W trend. Higher Au grades (Fig. 11c), correspond with areas where the V10 has an azimuth close to 300°, decreasing considerably when it turns to E-W trends. At grades higher than 50 ppm Au are concentrated in the sections with an average dip of 85°, while the lowest grades are distributed in areas where dip is less than 80°. The Ag grades behave in a similar way, those above 25 ppm are grouped in sectors of the vein with an azimuth of 300°, with a subvertical dip (85–90° average), while the lower grades tend to be located in the E-W oriented sections with a lower average dip (75°).

The V20 vein is the central structure of the Armadillo system (Fig. 12a), and like V10, exhibits different thickness distribution, and Au and Ag grades dependent on the vein attitude. The highest vein thickness occurs in the western and central sections of the vein, where it has an azimuth of between 290 and 300° (Fig. 12b), exhibiting a gradual decrease in thickness towards 280–290°, indicating less variation with respect to V10. This behavior also agrees with the Au (>50 ppm) and Ag (>50 ppm) distribution (Fig. 12c), which have higher composited grades over vein width where the structure shows an azimuth close to 300°,

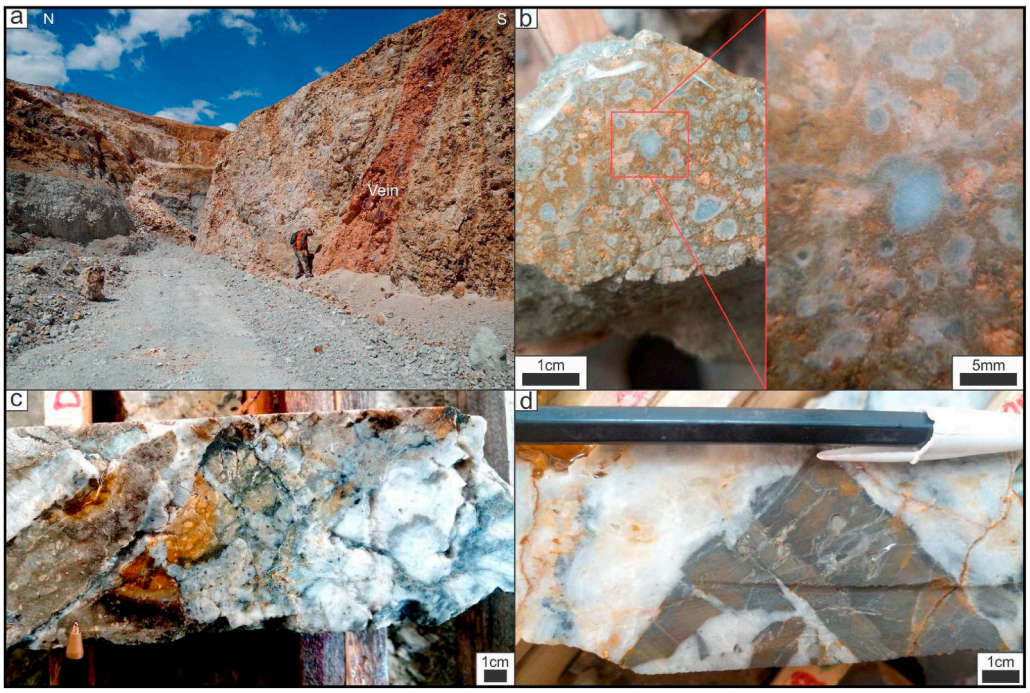

Fig. 14. **(a)** Quartz vein (red) cutting the rhyodacitic cryptodomes in the Armadillo pit. **(b)** Core sample photograph with quartz veinlets cutting the andesitic dyke and filling its vesicles (with low Au grade). **(c)** Core sample photograph, siliceous cement breccia affecting the matrix of the peperitic breccia of the Armadillo cryptocrypt rim. **(d)** Core sample photograph of the Armadillo sector showing a quartz cement breccia affecting the volcaniclastic sequence.

both decreasing considerably in the stretches of average azimuth 290°.

5.3. 3D vein analysis: CVZ

The thinner and close spacing between the veinlets makes it difficult to track individual veins in 3 dimensions, so to generate a 3D model we interpolated the logged structures from the diamond drillholes and reverse circulation drilling together with the structures mapped and analyzed at surface with a thickness of at least 25 cm within 461 drill holes and 1800 dip structural measurements of veinlets from mapping of open pits and trenches.

Using this method, 24 veins/veinlets of more than 25 cm in thickness were modeled, within which the Au content was evaluated (Fig. 13a and b). Of these, the orientations of the veins with the highest quantity of mapping structural data were subdivided by Au content in a stereographic diagram by they average Au grade (Fig. 13c and d). The stereogram shows a trend of highest gold concentration where the average azimuth of the structure is approximately 305°, decreasing its content as the strike diminishes to 290°.

In the model of Fig. 13b, it is seen that the highest metal values are found in the NW-trending parts of the veins and where veins intersect, defining optimal areas of permeability and dilation (Fig. 13d).

Fig. 13a and b, show multiple veins hosted by sets of parallel WNW faults. The veinlets show a main 300–320° orientation, with high Au grades in 305–310° (Fig. 13c and d), represented by fill faults with a mainly extensional with minimal strike slip displacement (Fig. 13e).

This pattern is interpreted as a WNW oblique normal faults with NW jogs and oblique fill faults intersection favoring the conformation of the mineralized ore shoots.

6. Lithological controls

A lithological control on mineralization corresponds to the lithologies with which the hydrothermal fluid interacts, since mechanical anisotropy can generate variations in fracture density, changes in the orientation of the structures, or a combination of both.

The distribution and geometry of mineralized structures responds largely to the competence and permeability of the units they pass through (Corbett, 2007), while their composition can play a fundamental role in the precipitation or concentration of metals in the deposit. Also, hydrothermal alteration within the epithermal environment can profoundly modify rock rheological properties, and therefore influence the distribution and geometry of mineralized structures (Rhys et al., 2020). In the following section, we describe two aspects of the controls that the host rock defines to the mineralization of the Martinetas district, from the permeability point of view and the reactivity of its components.

6.1. Permeability of host rocks

Shallow epithermal environments usually encompass large variations in the permeability of the geological units present, primary permeability is low in rocks with low interconnected intergranular porosity, such as densely welded ignimbrites, or coherent volcanic rocks, which forces the flow of hydrothermal fluids to be channeled through fractures (Cox et al., 2001; Corbett, 2007). In contrast, lithologies with high primary permeabilities, such as clastic and volcaniclastic sedimentary rocks, are usually hydraulically conductive.

The presence of impermeable and competent rocks within a lower competent and permeable rock can lead to the accumulation of hydrothermal fluids along contacts, resulting in large variations in fluid pressure (Pf). The Pf gradient can promote fracturing of the more competent rock in the zone of dilatancy created by the variation in such stress and thus trigger the opening of spaces, providing a potential site for mineralization (Phillips, 1972). Overpressure leading to fracturing is usually much easier to achieve along such boundaries than in homogeneous rock bodies.

The mineralized structure of the district comprises veins, sub-parallel veinlets and quartz cement breccias, whose distribution is closely influenced by the host rock. The southern sector of Martinetas includes Armadillo and Choique sectors, which are characterized by the presence of subvolcanic bodies hosted in the Phreatomagmatic sequence. The preferential host rock corresponds to the coherent rhyodacitic

Fig. 15. (a) Geological profile of the Coyote - Cerro Oro (CVZ) sectors integrating the model of mineralized structures and the ratio meters drilled/meters with mineralized structures in the pumiceous and eutaxitic facies, within the Martinetas ignimbrite.*The section has a radius of influence of 20 m for the drill holes. **(b)** Core photograph with quartz veinlets (Vn) cutting a fault breccia (FBx) in the eutaxitic facies (MI). **(c)** Photograph of the SE front of the Cerro Oro pit, showing the pumiceous facies of the Martinetas ignimbrite cut by subparallel veins (sheeted veins). For scale, the mining face is 5m high. **(d)** Coronal core photograph, Vein with colloform banded texture within the pumiceous facies.

subvolcanic unit and minor andesitic dykes, where the structure forms veins up to 5 m thick (Fig. 14a), and the host rocks exhibit intense silicification. The different physical characteristics of these units are related to changes in the type of the mineralization. This is reflected, for example, in the andesitic dyke, where the vesicles are filled by the mineralizing fluid when the quartz veinlets cut them (Fig. 14b). The rhyodacitic cryptodomes exhibit wider veins in its more coherent portions, while at the edges, where peperitic breccias and intrusive hyaloclastites are generated, the matrix is cemented with hydrothermal quartz (Fig. 14c). On the other hand, the Phreatomagmatic Sequence is restricted to lithic breccias of hydrothermal siliceous cement with varied size of skeletal clasts from the host rock itself (Fig. 14d). In contrast, in the northern sector of the Martinetas district, represented by the Cerro Oro and Coyote (CVZ) pits, the mineralization is characterized mainly by sheeted vein (Fig. 15). The host rock corresponds to the Martinetas ignimbrite, composed broadly by two facies, a eutaxitic facies at the base and another less welded (pumiceous) towards the top, exhibiting a gradual transition between them (Fig. 15a).

A transversal section shows a multiplication of the veinlets towards the surface from the aforementioned elevation (Fig. 15a). In order to quantify the veinlet volume in the rock at both levels, the ratio between meters of mineralized structure and meters drilled was calculated, which shows a participation of 0.8% of veinlets for the pumiceous facies and 0.4% for the eutaxitic facies (Fig. 15a). These discontinuity planes were used by the hydrothermal fluid for its ascent (Fig. 15b). The dense sheeted veins in the CVZ pit (Fig. 16c and d) can respond to two situations: (1) The mineralized bodies are mainly hosted in the disseminated adularia-quartz-altered zone, within the most permeable facies. (2) On the other hand, the ore is controlled by upward steeping of vein-hosting faults accompanied by branching into multiple parallel extensional veins (Sibson, 2000; Rhys et al., 2020).

6.2. *Reactivity of the host rock*

Another aspect to highlight as a lithological control of mineralization is the reactivity of the host rocks and their interaction with the hydrothermal fluid. Gold precipitation has been recorded by reduction processes linked to the presence of type III kerogens in siliceous pulses forming the veins (De Martino et al., 2020b).

Vitrinite macerals are derived from parenchymatous and woody tissues of roots, stems, bark and leaves composed of cellulose and lignin (ICCOP, 1998). Inertinite is considered to be derived from plant material that has been strongly altered and degraded under oxidizing conditions (Falcon and Snyman, 1986), which is associated with forest fires (Cope and Chaloner, 1985; Guo and Bustin, 1998; Glasspool, 2000) or subaerial oxidation (Gize, 1997). The latter may be evidence of carbonization pre or syn-deposition of the pyroclastic flow containing the carbonaceous debris. Kerogen is an insoluble organic component, which

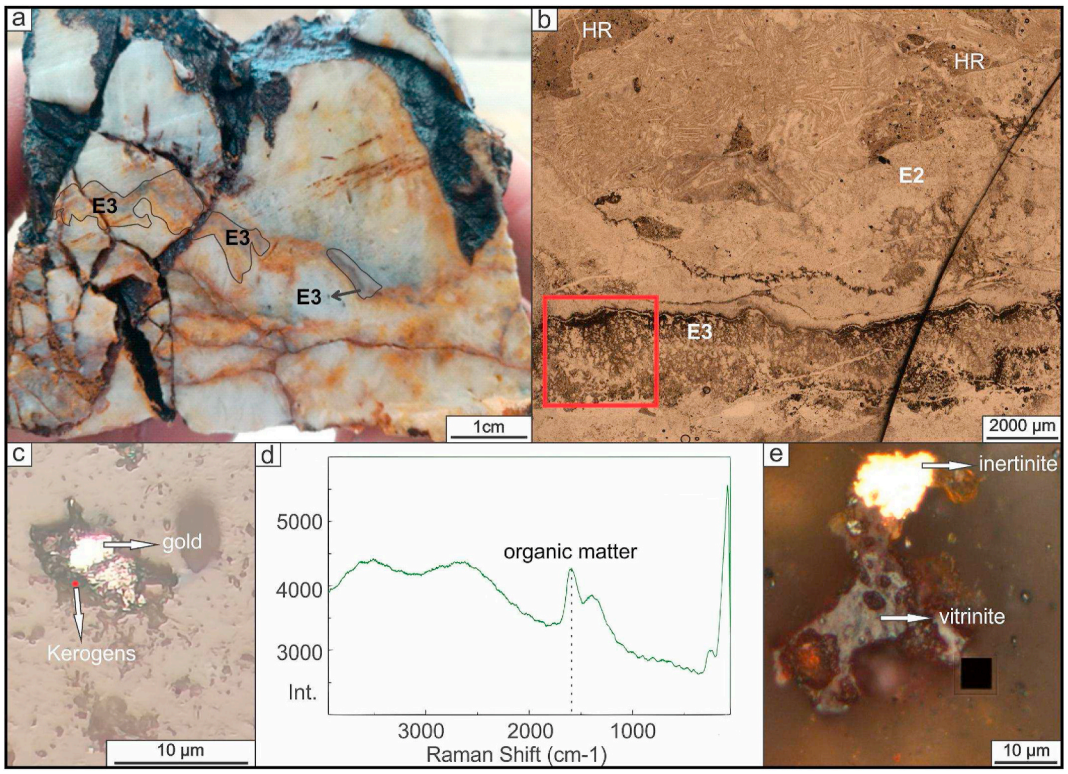

Fig. 16. **(a)** Hand sample photograph, where Event 3 of dark color is observed in the Armadillo system. **(b)** Photomicrograph with plane polarized light, black bands correspond to carbonaceous material in Pulse 3. The red box shows the sector where the detailed analyses of figures (c), (d) and (e) were performed. *HR: Host rock clasts.* **(c)** Photomicrograph under reflected light into the red box (figure b). The gold is surrounded by black material, the red dot indicates the sector where the Raman spectrometry was performed. **(d)** Spectral signature of Raman spectrometry in red dot (figure c), indicating the presence of organic matter (OM). **(e)** Vitrinite and inertinite observed in Pulse 3 under reflected light and oil immersion in sample of figure a.

implies its mobility as debris within the hydrothermal fluid that contains it (Hu et al., 1999).

The event E3 in the Armadillo vein system is characterized by the presence of gold-linked components of organic origin (Fig. 16a–c), determined from Raman microscopy (Fig. 16d). By analysis of these components under reflected light optical microscopy and oil immersion, it has been determined that they correspond to macerals of vitrinite and inertinite (Fig. 16e; De Martino et al., 2020b). Within the kerogen-loaded pulse (Event 3), gold grains are observed surrounded or attached to the organic debris (Fig. 16). Also, the distribution of hydrothermal events in the Armadillo veins (Fig. 17) demonstrate a close spatial relationship between the higher gold grades and the kerogen-loaded event.

The kerogen in the Armadillo veins may be genetically associated to a pyroclastic event causing the carbonization of the plants, which may be the deposits of the Phreatomagmatic Sequence with carbonaceous debris, as the older unit with this component observed in the sector (De Martino et al., 2017).

7. Discussion

7.1. Syn-mineral kinematics and structural control of mineralization

The permeability of the rock mass is a determining factor for the transport and deposition of mineralizing hydrothermal fluids. The circulation within a structure will depend mainly on the degree of fracturing of the host rock (Kim et al., 2003; Sibson, 1996). Main structures are usually relatively continuous and thicker, given the repetition of sliding caused by successive seismic events that concentrate on them, allowing the deposition of repeated hydrothermal pulses in the same structure (Blenkinsop, 2008). While transfer zones form damage sites and generate a greater number of thinner fractures. This property allows these sectors to contain high grades by concentrating fluid circulation (Seebeck et al., 2014; Sibson, 1996; Cox, 2005).

Generally, mineralized structures present a heterogeneous metal content distribution, where the zones with higher contents are called mineralized ore shoots (Nelson, 2006) and usually constitute the sectors of greater localized opening within the structure, so they usually coincide with the thickest portions within the structure, coinciding with curvatures or jogs (Corbett, 2007). Although ore shoots may occur at branch lines and dilatational jogs along the main fault strand and in the extensional relays and upwars-bifurcating dilatational fans in normal faults, as well as interactions between structures of different ages (Rhys et al., 2020); in stress controlled vein systems, the orientation of these ore shoots is controlled by the direction of slip of the blocks bounding the structure, which is controlled by the orientation of the principal stress field ($\sigma1 > \sigma2 > \sigma3$; Poulsen and Robert, 1989). The last case allows us to predict ore shoots positions and geometry with an accurate kinematic interpretation of controlling faults.

From the analysis of the Armadillo and Central Vein Zone sectors, it has been possible to determine the preferential orientations of the structures for the highest metal contents in the Martinetas district.

In order to analyze in detail the relationship between the geometry of the structure with the Au content and to complement the study of the structural disks carried out in both Armadillo and CVZ (Figs. 11–13), the information obtained in the 3D structural model generated from the map of the open pit mine and logged drill holes was graphically arranged. The northern structure of the Armadillo vein system was chosen as it contained the most information (Fig. 18a).

The veins present in Armadillo have a general WNW orientation, with thicker segments of NW trend and strong dip to the NE. Secondarily, there are sections of ENE orientation and strong dip to the south,

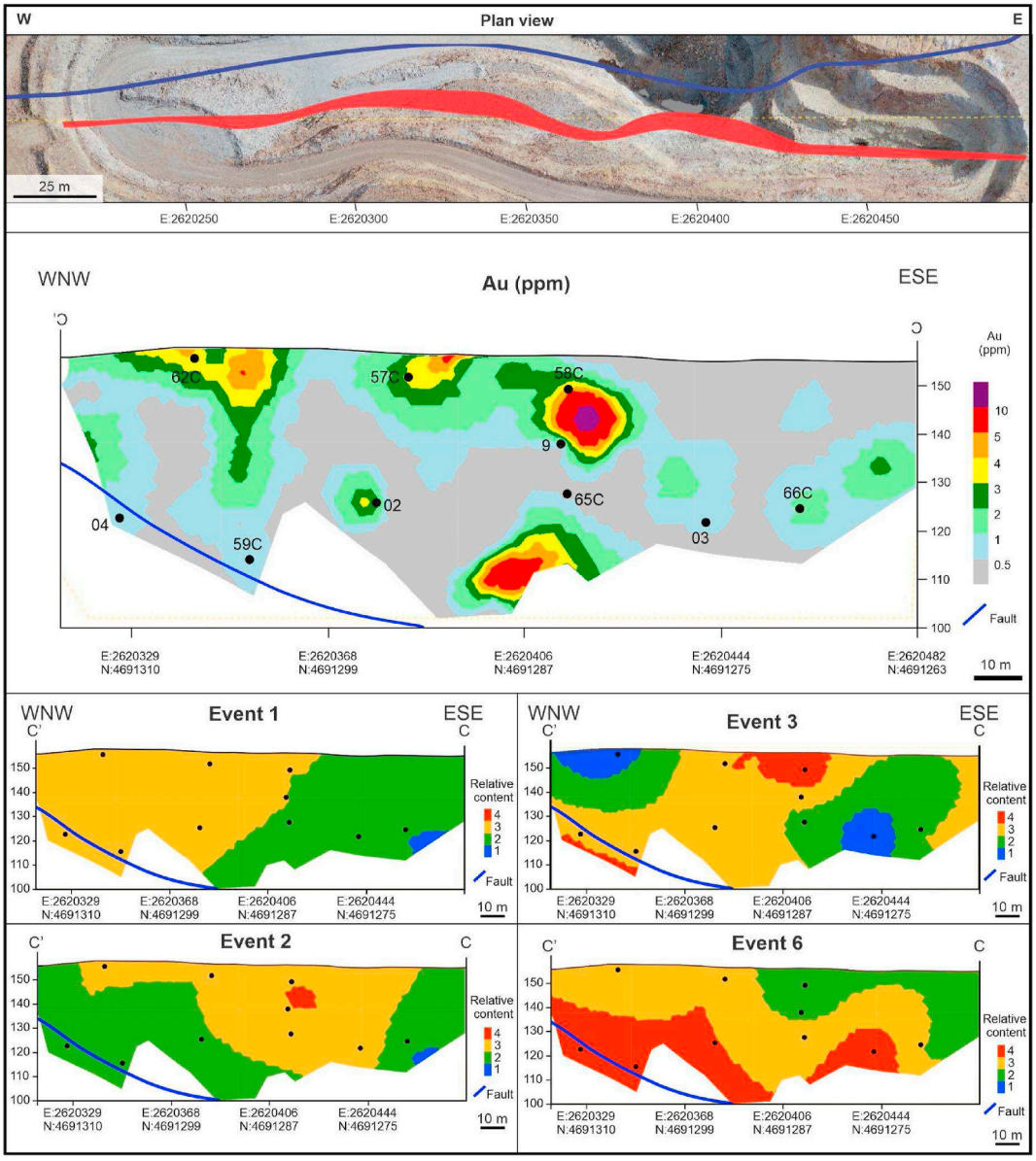

Fig. 17. Longitudinal section of the main vein in the Armadillo sector (Fig. 3.3), showing the distribution of Au values and the relative abundance of the structure-forming events. The black dots indicate the diamond drill holes used to model the distribution of the events (hole ID in Au profile).

where the structure has less thickness. The grades are distributed following the NW to WNW segments, constituting mineralized ore shoots with a subvertical dip where the structure presents a NW orientation, inclining 45° to the NW where the structure presents flexures with this orientation, while the ENE azimuth sections present low grades (Fig. 18b). The distribution of Au content in the vein coincides with its thicknesses, as shown in Fig. 18c, the NW oriented segments exhibit up to 7m of thickness, representing the sectors of greater openness, while, in the ENE segment its thickness is reduced to less than 1 m, representing the closure of the structure. The latter is related to the kinematics of the blocks containing the vein. This arrangement of ore shoots is compatible with the σ3 oriented N35°E, as estimated for the study area from sigmoids and slickenlines. This results in an oblique normal-dextral syn-mineral kinematics for the NW oriented sections (oblique ore shoots) and a greater component of movement in the direction (dextral) where the vein has a WNW azimuth (vertical ore shoots).

Although this geometrical analysis is difficult for CVZ, given the low thickness and continuity of the veinlets present there, the statistical analysis performed for that sector from the generation of structural disks (Fig. 13c and d), allowed determining an azimuth of 306° as the orientation with the highest Au contents within the veinlets, with a reduction in the average grade as the veinlets exhibit an E-W orientation. This pattern is similar to that of Armadillo, so it is considered that the orientation of the syn-mineral stress field is the same in both sectors.

7.2. *Host rocks and lithological control of mineralization*

Low and intermediate sulfidation epithermal deposits often develop predominantly in dilational structures, e.g., Amancaya (Lopez et al., 2018), Martha mine (Páez et al., 2011) and Manantial Espejo (Echeveste, 2010). At other times, fluids are deposited by moving from host structures in impermeable to permeable lithology (e.g., Maragorik; Corbett and Hayward, 1994), where the intersection of extensional structures with permeable horizon planes represent ideal environments for fluid deposition (Corbett, 2002). Thus, structural control commonly extends from major structural corridors that localize the mineral system to second- or third-order fractures with lithologic control.

Mineralized structures in the district include veins, isolated veinlets,

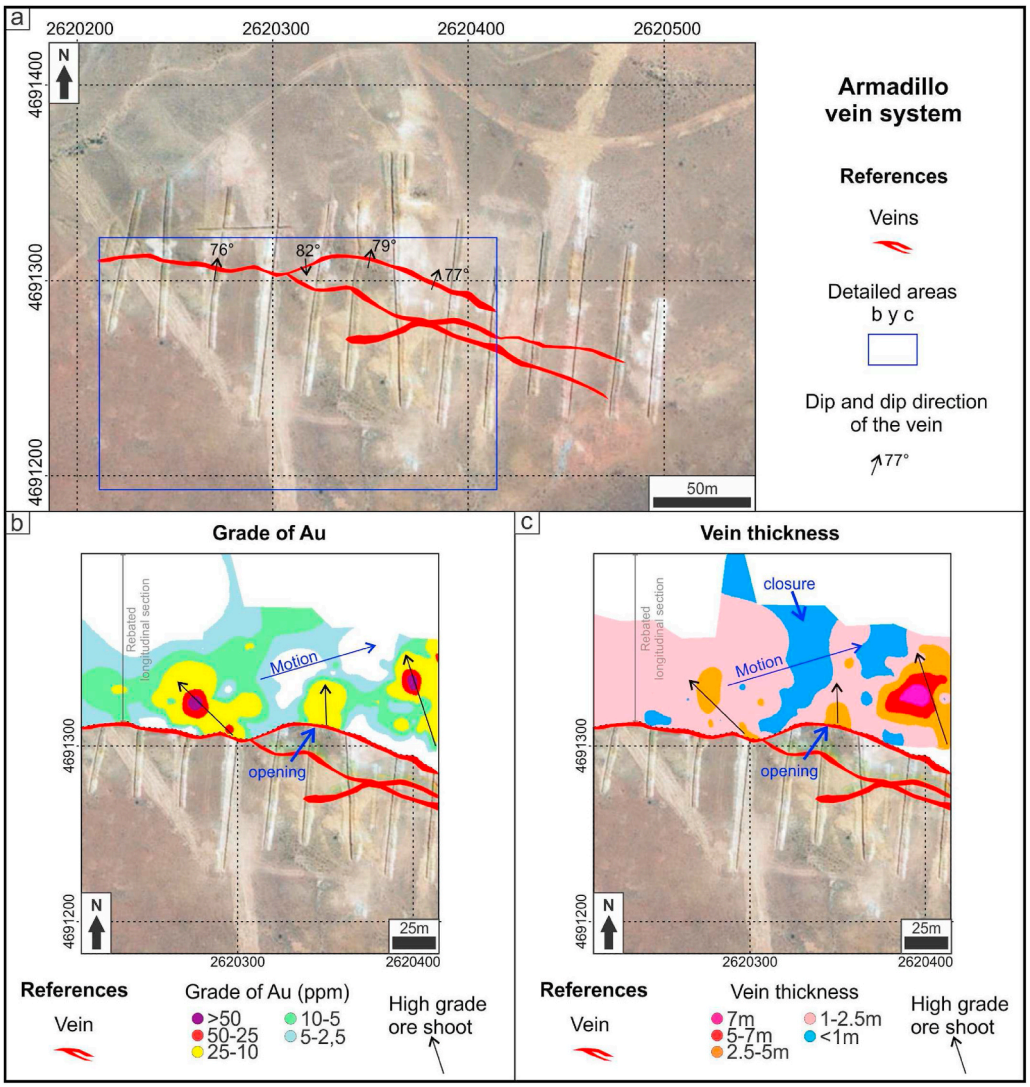

Fig. 18. **(a)** Location map of the Armadillo vein system. **(b)** Plan view map of longitudinal section with grade distribution within the northern Armadillo vein with direction of opening, perpendicular to NW jogs. *Black arrows indicate the inclination of the ore shoots within the vein. **(c)** Plan view map of longitudinal section showing the thickness distribution of the north Armadillo vein with the direction of opening and syn-mineral movement of the structure.

closely spaced sub-parallel veins (sheeted veins) and hydrothermal injection breccias. These patterns have a distribution strongly controlled by the lithology hosting the structure.

In shallow epithermal environments there are often large variations in permeability (k) between and within geological units, such as in ignimbrites with variation in their degree of welding, whose permeability can vary by a factor of 10^4, (Ingebritsen and Manning, 2010). Although according to John et al. (2018), primary permeability is low in rocks with low interconnected intergranular porosity (k less than 10–16/m^2), such as densely welded ignimbrites and coherent magmatic rocks, and hydrothermal fluid flow depends on secondary permeability; and lithologies with high primary permeabilities (k greater than 10–16/m^2), such as in unwelded ignimbrites and poorly cemented clastic rocks, hydrothermal fluids flow through them in response to fluid pressure gradients. Once altered the mechanical and permeability characteristics of the rocks will change.

Therefore, it is interpreted that in the rhyodacitic and andesitic subvolcanic rocks that characterize the south of the district, fluid ascent would be controlled by fracture permeability (Cox et al., 2001; Ingebritsen and Manning, 2010; Rowland and Simmons, 2012). Similarly, the Martinetas Ignimbrite's pumiceous facies allowed the hydrothermal fluids a wide dispersion of quartz-adularia alteration, which, along with the upward steeping of vein-hosting faults accompanied by branching into multiple parallel extensional veins that localized ore shoots. Whereas, in the poorly cemented or welded clastic rocks of the district, represented by the Phreatomagmatic Sequence and the edge breccias of the rhyodacitic Cryptodome, the ascent of fluids would clearly respond to their pressure gradients, generating breccias by injection of the hydrothermal fluid.

On the other hand, from the compositional point of view of the bedrock, a close relationship has been determined between the organic matter present in the veins and the higher metal contents. The association of organic matter with mineral deposits, gangue and bedrock in low (<120°) and moderate (120–350°) temperature hydrothermal deposits is a well-studied and recognized phenomenon since the beginning of the 20th century (Harder, 1919; Schneiderholm, 1923; Saxby, 1976; Campbell, 1993; Parnell et al., 1993; Giordano, 1996; Leventhal and Giordano, 1997; Gize, 1999; Kettler, 2000; Pirajno, 2009).

Kerogens and their derivatives (bitumen, pyrobitumen) can act in different ways in the formation of a metalliferous deposit. According to Leventhal and Giordano (1997), organic matter and its derivatives can have six active roles in the processes that form or preserve metalliferous deposits. These can be: 1- Mobilization (when the source of metals are linked to surface rocks and sedimentary environments, anomalies are

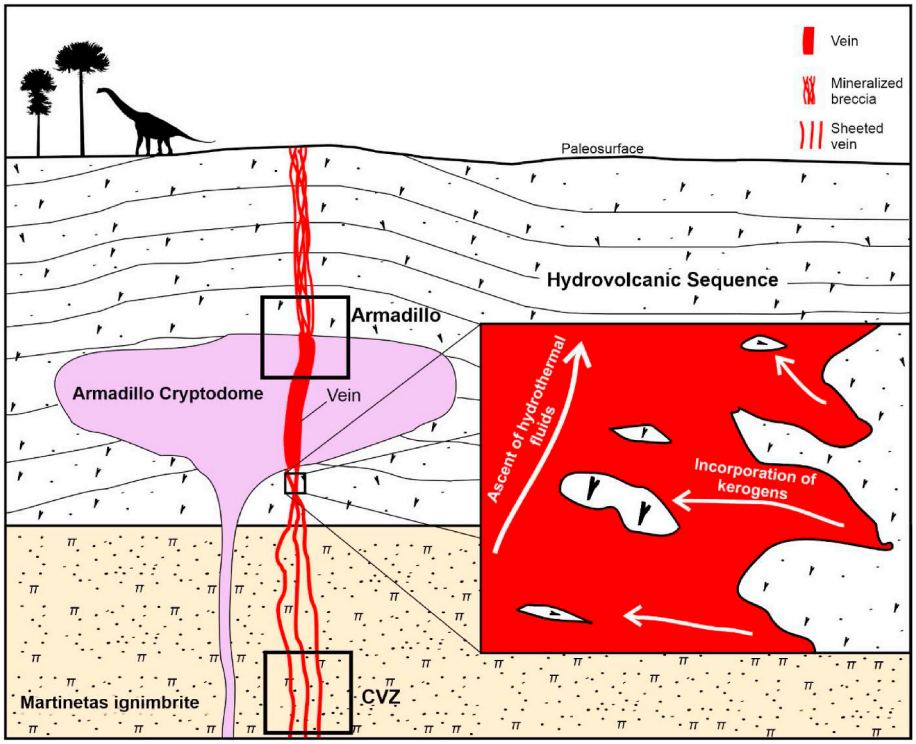

Fig. 19. Schematic representation in profile of the ascent of the hydrothermal fluid through rocks with high carbonaceous content and incorporation of the kerogens it contains.

associated with dissolved organic matter), 2-Transport (by organic metal complexes in groundwater and hydrothermal fluids), 3- Concentration (metals in the deposit are better correlated with organic matter than with sulfides), 4- Reduction (there is partially oxidized organic matter and both metals and sulfides correlate with organic matter concentrations, autochthonous kerogen can serve as a reductant for metals and sulfides), 5- Oxidation (by microorganism activity), 6- Preservation (mineral grains surrounded or covered by micro or macroscopic organic matter). Considering this, organic matter playing some role in the genesis of a deposit can be used as an exploratory tool (Levinson, 1974; Rose et al., 1979; Carlisle et al., 1986; Landis and Hofstra, 1991; Brooks et al., 1995; Leventhal and Giordano, 1997).

Since there is a correlation between the anomalous gold values in Event 3 and the concentration of organic matter within these pulses, and the grains of gold are covered by kerogen, a relationship between precious metal precipitation and organic matter is interpreted. Kerogen would be one of the direct (Au fixation by lignite) or indirect (reduction by bacteria or thermochemically induced by changes in fluid Eh and pH by organic matter) responsible for gold precipitation (Leventhal and Giordano, 1997). This would involve the passage of the hydrothermal fluid through carbonaceous levels (Pheatomagmatic Sequence or another unit below the volcanic sequence) and the uptake of the kerogens it contains, causing the subsequent reduction and precipitation of the metal (Fig. 19). The organic material is derived from deep hydrothermal circulation through rocks with high carbonaceous content.

Although the boiling of the hydrothermal fluid is understood to be the main process driving the deposition of metals in the Martinetas district, it is interpreted that the carbonaceous debris present in the Armadillo veins migrated as a result of the hydrothermal event responsible for the generation of the metals, playing a secondary role as a reducing or preserving agent for gold, increasing the grades where they are present (De Martino et al., 2020b).

8. Conclusions

The Martinetas district has two distinct sectors from the point of view of the geometry of the mineralized structure and the permeability and competence of the host rocks. The southern portion of the district is represented by the Armadillo and Choique sectors, whose preferential hostrocks correspond to coherent subvolcanic units of rhyodacitic and andesitic composition, where the mineralized structure forms a WNW corridor with NW oriented sigmoid and flexures, where it exhibits the highest metal concentrations. Secondarily, clastic rocks adjacent to these subvolcanic bodies present scarce mineralized structures, mainly represented by mineralized quartz cement breccias. On the other hand, the northern half of the district, represented by the Coyote and Cerro Oro sectors is characterized by a dense concentration of subparallel veinlets of few centimeters of thickness, hosted in an ignimbrite composed of two facies with different degree of welding. The lower facies is eutaxitic and contain minor dispersion of quartz-adularia-illite alteration and lower density of veinlets than the pumiceous facies above it. This distribution is associated with the primary permeability differences, modified by syn-mineral alteration, in addition to upward steepening, branching and dilation of extensional fault hosted vein system near surface. The deflection and bifurcation of faults became important permeable fluid conduits and dilational sites during vein formation.

The highest Au and Ag grades in Armadillo and CVZ are concentrated in the thickest, most dilatant vein sections, implying an extensional vector of approximately N35°E orientation. From the geometric arrangement observed in both vein systems, it is interpreted that the active tectonic environment at the time of operation of the hydrothermal system corresponds to an oblique extensional regime characterized by normal-dextral kinematics.

On the other hand, gold was mainly enriched in insoluble organic matter-kerogen and a close relationship has been determined between the kerogens present in the veins and the higher metal contents.

CRediT authorship contribution statement

Facundo.J. De Martino: Conceptualization, Investigation, Methodology, Project administration, Resources, Software, Writing – original draft. **Sebastián M. Jovic:** Conceptualization, Funding acquisition, Investigation, Methodology, Software, Writing – original draft. **Luciano López:** Funding acquisition, Validation, Visualization, Writing – review & editing. **Horacio J. Echeveste:** Validation, Writing – review & editing.

Declaration of competing interest

The authors declare that they have no known competing financial interests or personal relationships that could have appeared to influence the work reported in this paper.

Acknowledgements

This research is part of F.J. De Martino PhD thesis and was funded through a CONICET PhD grant, the generous logistical support of Minera Don Nicolás S.A. and additional funds from the UNLP Grant N797 entitled "Controles volcánico y tectónico de mineralizaciones epitermales jurásicas del Macizo del Deseado". The authors want to give a special thank to Cerrado Gold inc. and the mine's exploration team for providing access to information and drill-cores, for their valuable discussions and input on the local geology and also for encouraging the publication of this work.

We would also like to thank David Rhyce and Leandro Echavarría for their valuable contributions.

References

Ameghino, F., 1898. Sinopsis Geológico-Paleontológica (Formaciones Cenozoicas Y Cretáceas). Segundo Censo de la República Argentina, pp. 113–255, 1895), Tomo 1.

Archangelsky, S., 1958. Estudio geológico y paleontológico del Bajo de la Leona, Santa Cruz. Acta Geol. Lilloana 2, 5–133 (San Miguel de Tucumán).

Arrondo, O.G., 1972. Estudio geológico y paleontológico de la zona de Estancia La Juanita y alrededores, provincia de santa Cruz, Argentina. Paleontología 43, 1–194. Revista del Museo de La Plata (nueva serie).

Blenkinsop, T., 2008. Relationships between faults, extension fractures and veins, and stress. J. Struct. Geol. 30, 622–632. https://doi.org/10.1016/j.jsg.2008.01.008.

Brooks, R.R., Dunn, C.E., Hall, G.E.M., 1995. Biological Systems in Mineral Exploration and Processing. Ellis Horwood, London, p. 538.

Browne, P.R.L., Ellis, A., 1970. The Ohaki-Broadlands hydrothermal area, New Zealand: Mineralogy and related geochemistry. Am. J. Sci. 269, 97–131.

Campbell, W.R., 1993. Research drilling into the creede epithermal vein system, San Juan mountains, Colorado. Soc. Econ. Geol. Newslett. 13 (1), 12–16.

Carlisle, D., Berry, W.L., Kaplan, I.R., Watterson, J.R., 1986. Mineral Exploration: Biological Systems and Organic Matter. Prentice-Hall, Englewood Cliffs, p. 465 (New Jersey).

Cline, J.S., Hofstra, A.H., Muntean, J.L., Tosdal, R.M., Hickey, K.A., 2005. Carlin-type Gold Deposits in Nevada-Critical Geologic Characteristics and Viable Models. Economic Geology 100th Anniversary, pp. 451–484.

Cope, M.J., Chaloner, W.G., 1985. Wildfire, an interaclion of biological and physical processes. In: Tiffney, B.H. (Ed.), Geological Factors and the Evolution of Plants. Yale University Press, Hartford, CT, pp. 257–277.

Corbett, G.J., 2007. Controls to low sulphidation epithermal Au-Ag: Charla presentada in una reunión del Grupo de Discusión de Exploración Mineral de Sydney (SMEDG), powerpoint and texto in el sitio web del SMEDG. http://www.smedg.org.au.

Corbett, G., 2002. Epithermal Gold for Explorationists. Australian Institute of Geoscientists Journal - Applied Geoscientific Practice and Research in Australia.

Corbett, G.J., Hayward, S.B., 1994. The Maragorik high sulphidation Cu/Au system - an update. In: Rogerson, R. (Ed.), Geology, Exploration and Mining Conference, June 1994, Lae, Papua New Guinea, Proceedings: Parkville. The Australasian Institute of Mining and Metallurgy, pp. 125–129.

Cowan, E.J., Beatson, R.K., Ross, H.J., Fright, W.R., McLennan, T.J., Evans, T.R., Carr, J. C., Lane, R.G., Bright, D.V., Gillman, A.J., Oshust, P.A., Titley, M., 2003. Practical implicit geological modelling. In: 5th International Mining Geology Conference, 8, pp. 89–99.

Cox, S.F., 2005. Coupling between Deformation, Fluid Pressures and Fluid Flow in Ore-Producing Hydrothermal Environments. Economic Geology 100th Anniversary, pp. 39–75.

Cox, S.F., Knackstedt, M.A., Brown, J., 2001. Principle of structural control on permeability and fluid flow in hydrothermal systems. In: Richards, J.P., Tosdal, R.M. (Eds.), Structural Control on Ore Genesis: Reviews in Economic Geology, vol. 14, pp. 1–24.

De Martino, F.J., 2021. Investigación sobre el control estructural y litológico de la mineralización en el prospecto de oro y plata Martinetas, sector oriental del Macizo del Deseado, provincia de Santa Cruz. Tesis Doctoral Universidad Nacional de La Plata. Inédita, p. 209.

De Martino, F.J., Paez, G., Echeveste, H., Jovic, S.y., Tessone, M.O.R., 2020a. Felsic magma-water interaction in shallow intrusive environments: timing between fluidal peperites and intrusive hyaloclastites in a jurassic cryptodome from the eastern Deseado Massif (patagonia, Argentina). J. S. Am. Earth Sci. 102654. https://doi.org/10.1016/j.jsames.2020.102654.

De Martino, F.J., Jovic, S.M., Echeveste, H.J., Tessone, M.O.R., Palma, D., 2020b. Precipitación de Au vinculada a materia orgánica. sistema vetiforme armadillo, mina Don Nicolas, Macizo del Deseado. Revista de la Asociación Geológica Argentina, vol. 77. Asociación Geológica Argentina, Buenos Aires, pp. 1851–8249 n°2. p-. issn 0004-4822. e-issn.

De Martino, F.J., Echeveste, H.J., Jovic, S.M., Tessone, M.O.R., 2017. Estratigrafía volcánica bimodal de los proyectos Martinetas and Microondas, sector oriental del Macizo del Deseado, Santa Cruz, Argentina. XX Congreso Geológico Argentino, Actas ST9, pp. 34–38.

Echeveste, H., 2010. Control estructural de la mineralización epitermal del distrito Manantial Espejo, Santa Cruz, Argentina. Rev. Asoc. Geol. Argent. 66, 325–334. http://www.scielo.org.ar/scielo.php?script=sci_arttext&pid=S0004-48222010000200004&lng=es&nrm=iso. Retrieved from.

Falcon, R., Snyman, C., 1986. An Introduction to Coal Petrology: Atlas of Petrographic Constituents in the Bituminous Coals of Southern Africa. The Geological Society of South Africa. Review paper Number 2. 9-13 pp.

Faulds, J.E., Coolbaugh, M.F., Hinz, N.H., 2011. Structural investigations of Great Basin geotermal fields—applications and implications. In: Steininger, Roger, Pennell, Bill (Eds.), Proceedings of the Great Basin Evolution and Metallogeny Symposium. Geological Society of Nevada, Reno, pp. 361–372, 2010.

Féraud, Alric, V., Fornari, M., Bertrand, H., Haller, M., 1999. $^{40}Ar/^{39}Ar$ dating of the Jurassic volcanic province of Patagonia: migrating magmatism related to Gondwana break-up and subduction. Earth Planet. Sci. Lett. 172, 83–96.

Fernández, M.L., Mazzoli, S., Zattin, M., Savignano, E., Genge, M., Tavani, S., Garrone, A., Franchini, M., 2019. Structural controls on jurassic gold mineralization, and cretaceous-tertiary exhumation in the foreland of the southern Patagonian Andes: new constraints from La paloma area, Deseado Massif, Argentina. Tectonophysics 775, 228302. https://doi.org/10.1016/j.tecto.2019.228302.

Feruglio, E., 1949. Descripción geológica de la Patagonia. Dirección General de Yacimientos Petrolíferos Fiscales, Tomo II, p. 349 (Buenos Aires).

Fracchia, D., Giacosa, R., 2006. Evolución estructural del basamento ígneo-metamórfico in la estancia Las Tres Hermanas, noreste de la Comarca del Deseado, Santa Cruz. Rev. Asoc. Geol. Argent. 61 (1), 118–131.

Fuchs, S., Schumann, D., Williams-Jones, A., Murray, A., Couillard, M., Lagarec, K., Phaneuf, M., Vali, H., 2017. Gold and uranium concentration by interaction of immiscible fluids (hydrothermal and hydrocarbon) in the Carbon Leader Reef, Witwatersrand Supergroup, South Africa. Precambrian Res. 293 https://doi.org/10.1016/j.precamres.2017.03.007.

Giacosa, R., 2020. Basement control, sedimentary basin inception and early evolution of the Mesozoic basins in the Patagonian foreland, 2020 J. S. Am. Earth Sci. 97, 102407. https://doi.org/10.1016/j.jsames.2019.102407. ISSN 0895-9811.

Giacosa, R., Zubia, M.A., Sánchez, M., Allard, J., 2010. Meso-Cenozoic tectonics of the southern Patagonian foreland: structural evolution and implications for Au–Ag veins in the eastern Deseado Region (Santa Cruz, Argentina). J. S. Am. Earth Sci. 30 (3–4), 134–150.

Giacosa, R., Márquez, M., Panza, J., 2002. Basamento Paleozoico inferior del Macizo del Deseado. Relat. 15 Congr. Geol. Argent. 33–44.

Giordano, T.H., 1996. Special issue on organics and ore deposits. Ore Geol. Rev. 11 (1–3), 173.

Gize, A., 1999. Organic alteration in hydrothermal sulfide ore deposits. Econ. Geol. 94, 967–980.

Gize, A., 1997. "Organic Petrology applied to ore deposits" in ore genesis and exploration: the roles of organic matter. Rev. Econ. Geol. 9, 63–83.

Glasspool, I.J., 2000. Megaspores from the late Permian, lower whybrow coal seam, Sydney basin, Australia. Rev. Palaeobot. Palynol. 110, 209–227.

Godeas, 1992. Geoquímica y marco tectónico de los granitoides en el Bajo de la Leona (Formación La Leona), provincia de Santa Cruz. Revista Asociación Geológica Argentina 47, 333–341.

Guido, D., 2004. Subdivisión litofacial e interpretación del volcanismo jurásico (Grupo Bahía Laura) in el este del Macizo del Deseado, provincia de Santa Cruz. Rev. Asoc. Geol. Argent. 59 (4), 727–742.

Guido, D.M., Campbell, K.A., 2011. Jurassic hot spring deposits of the Deseado Massif (Patagonia, Argentina): characteristics and controls on regional distribution. J. Volcanol. Geoth. Res. 203, 35–47.

Guo, Y., Bustin, R.M., 1998. Micro-FTIR spectroscopy of liptinite macerals in coal. Int. J. Coal Petrol. 36, 259–275.

Haller, M.J., 2002. La cuenca triásica de El Tranquilo. En. In: Haller, M.J. (Ed.), Geología y recursos Naturales de Santa Cruz. Relatorio del XV Congreso Geológico Argentino, pp. 83–88.

Harder, E.C., 1919. Iron-depositing bacteria and their geologic relations: U.S. Geological Survey Professional Paper 113: 89 p. International Committee for Coal and Organic Petrology (ICCP) 1998. The new vitrinite classification (ICCP system 1994). Fuel 77, 349–358.

Hechem, J.J., y Homovc, J.F., 1987. La relación entre las Formaciones Baqueró y Laguna Palacios en el Nesocratón del Deseado, provincia de Santa Cruz. Rev. Asoc. Geol. Argent. 42, 244–254.

Hedenquist, J., Arribas, A., 2019. Environments of advanced argillic alteration I. Mineral stability and hypogene formation II. Steam-heated, supergene, and exploration implications. In: Conference paper: Society of Resource Geology of Japan, Annual Meeting, At Tokyo, Japan, p. 69.
Hedenquist, J.W., Arribas Jr., A., Urien-Gonzalez, E., 2000. Exploration for epithermal gold deposits. In: Hagemann, S.G., Brown, P.E. (Eds.), Gold in 2000: Society of Economic Geologists, Reviews in Economic Geology, vol. 13, pp. 245–277.
Henley, Truesdell, A.H., Barton, P.B., Whitney, J.A., 1984. Fluid-mineral equilibria in hydrothermal systems. Rev. Econ. Geol.
Herbst, R., 1965. Algunos esporomorfos del Triásico de Argentina. Ameghiniana 4, 141–155.
Homovc, J.F., Constantini, L., 2001. Hydrocarbon exploration potential within intraplate shear-related depocenters: Deseado and San Julian basins, southern Argentina. AAPG (Am. Assoc. Pet. Geol.) Bull. 85, 1795–1816.
Hu, K., Zhai, J., Liu, Y., Wang, H., 1999. Kerogen-as a sort of organic bearer of gold in gold-bearing formations. Chin. Sci. Bull. 44 (11), 1045–1050. https://doi.org/10.1007/bf02886028.
Ingebritsen, S.E., Appold, M.S., 2012. The physical hydrogeology of ore deposits. Econ. Geol. 107, 559–584.
Ingebritsen, S.E., Manning, C.E., 2010. Permeability of the continental crust—dynamic variations inferred from seismicity and metamorphism. Geofluids 10, 193–205.
International Committee for Coal and Organic Petrology (ICCOP), 1998. The new vitrinite classification (ICCP System, 1994). Fuel 77, 349–358.
John, D.A., Vikre, P.G., du Bray, E.A., Blakely, R.J., Fey, D.L., Rockwell, B.W., Mauk, J.L., Anderson, E.D., Graybeal, F.T., 2018. Descriptive models for epithermal gold-silver deposits: U.S. Geological Survey Scientific Investigations Report 2010–5070–Q, 247. https://doi.org/10.3133/sir20105070Q.
Jovic, S., Guido, D., Sanchez, M., Páez, G., Ruiz, R., Permuy, C., López, L., 2014. Controles estructurales multi-escala en los sistemas epitermales del Macizo del Deseado. XIX Congreso Geológico Argentino, Córdoba.
Kay, S.M., Ramos, V., Mpodozis, C., y Sruoga, P., 1989. Late paleozoic to jurassic silicic magmatism at the Gondwana margin: analogy to the middle proterozoic in north America? Geology 17, 324–328.
Kettler, R.M., 2000. The interaction of organic matter and fluids during the genesis of some precious metal and volcanogenic massive sulfide deposits. Rev. Econ. Geol. 9, 301–313.
Kim, Y.-S., Peacock, D.C.P., Sanderson, D.J., 2003. Strike-slip faults and damage zones at Marsalforn, Gozo island, Malta. J. Struct. Geol. 25, 793–812.
Kokelaar, 1982. Fluidization of wet sediments during the emplacement and cooling of various igneous bodies. J. Geol. Soc. London 139, 21–33.
Landis, G.P., Hofstra, A.H., 1991. Fluid inclusion gas chemistry as a potential minerals exploration tool: case studies from Creede, CO, Jerritt Canyon, NV, Coeur d' Alene district, ID and MT, southern Alaska mesothermal veins, and mid-continent MVT's. J. Geochem. Explor. 42, 25–59.
Large, R., Bull, S., Maslennikov, V., 2011. A carbonaceous sedimentary source-rock model for carlin-type and orogenic gold deposits. Econ. Geol. 106, 331–358. https://doi.org/10.2113/econgeo.106.3.331.
Leventhal, A.G., Giordano, T.H., 1997. The nature and roles of organic matter associated with ores and ore-forming systems: an introduction. In: Giordano, T.H., Kettler, R. M., Wood, S.A. (Eds.), Ore Genesis and Exploration: the Roles of Organic Matter. Reviews in Economic Geology, vol. 9, pp. 1–26 (Littleton).
Levinson, A.A., 1974. Introduction to Exploration Geochemistry. Applied Publishing Ltd., p. 924 (Wilmette).
Lopez, P., Jovic, S., López, L., Paez, G., Guido, D., 2018. Marco and control estructural del depósito epitermal Amancaya, Antofagasta, Chile. XV Congreso Geológico Chileno.
Márquez, Massaferro, G.I., Fernández, M.I., Menegatti, N., Navarrete, C.R., 2011. El centro volcánico Sierra Grande: caracterización petrográfica y geoquímica del magmatismo extensional liásico, noroeste de la Patagonia. Revista de la Asociación Geológica Argentina 68 (4), 555–570.
McCoss, A.M., 1986. Simple constructions for deformation in transpression/ transtension zones. J. Struct. Geol. 8 (6), 715–718.
Micklethwaite, S., 2009. Mechanisms of faulting and permeability enhancement during epithermal mineralization-Cracow goldfield, Australia. J. Struct. Geol. 31, 288–300.
Navarrete, C., Gianni, G., Encinas, A., Márquez, M., Kamerbeek, Y., Valle, M., Folguera, A., 2019. Triassic to Middle Jurassic geodynamic evolution of southwestern Gondwana: from a large flat-slab to mantle plume suction in a rollback subduction setting. Earth Sci. Rev. https://doi.org/10.1016/j.earscirev.2019.05.002.
Nelson, E.P., 2006. Drill-hole design for dilational ore shoot targets in fault-fill veins. Econ. Geol. 101, 1079–1085.
Páez, G.N., Ruiz, R., Guido, D.M., Jovic, S.M., Schalamuk, I.B., 2011. Structurally controlled fluid flow: high-grade silver ore-shoots at Martha epithermal mine, Deseado Massif, Argentina. J. Struct. Geol. 33, 985–999.
Pankhurst, Leat, P.T., Sruoga, P., Rapela, C.R., Marquez, M., Storey, M., Riley, T.R., 1998. The Chon Aike province of Patagonia and related rocks in West Antarctica: A silicic large igneous province. J. Volcanol. Geotherm. Res. 81, 113–136.
Pankhurst, R., Riley, T.R., Fanning, C.M., Kelley, S., 2000. Episodic silicic volcanismin Patagonia and the Antarctic Peninsula: chronology of magmatism associated with the break-up of Gondwana. J. Petrol. 41, 605–625. https://doi.org/10.1093/petrology/41.5.605.
Pankhurst, R.J., Sruoga y, P., Rapela, C.W., 1993. Estudio geocronológico Rb-Sr de los Complejos Chon Aike y El Quemado a los 47°30' L.S. 12° Congreso Geológico Argentino. Actas 4, 171–178.
Panza, J.L., 1982. Descripción geológica de las Hojas 53e Gobernador Moyano y 54e Cerro Vanguardia. Servicio Geológico Nacional (inédito), Buenos Aires, p. 197.
Parnell, J., Hucha, H., Landais, P., 1993. Bitumens in Ore Deposits. Springer, New York, p. 520.
Phillips, W.J., 1972. Hydraulic fracturing and mineralisation. J. Geol. Soc. Lond. 128, 337–359.
Pirajno, F., 2009. Hydrothermal Processes and Mineral Systems. Springer, New York, p. 1250.
Poulsen, K.H., Robert, F., 1989. Shear zones and gold: practical examples from the southern Canadian Shield. In: Burnsall, J.T. (Ed.), Mineralization and Shear Zones: Geological Association of Canada, Short Course Notes, vol. 6, pp. 239–266.
Ramos, V.A., 2008. Patagonia: a Paleozoic continental rift? J. South Am. Earth Sci. 26, 235–251.
Ramos, V.A., Kay, S.M., 1992. Southern Patagonian plateau basalts and deformation: back-arc testimony of ridge collisions. Tectonophysics 205, 261–282.
Rapela, C.W., Pankhurst, R.J., 1996. Monzonite suites: the innermost cordilleran plutonism of patagonia. Earth Sci. 87, 193–203. Transactions Of The Royal Society Of Edinburgh.
Rapela, C.W., Pankhurst, R., 1992. The granites of northern patagonia and the gastre fault system in relation to the break-up of Gondwana. In: En, Storey, B., Alabaster, T., Pankhurst, R. (Eds.), Magmatism and the Causes of Continental Break-Up, vol. 68. Geological Society Special Publications, pp. 209–220.
Rapela, C.W., Días, G., Franzese, J., Alonso, G., Benvenuto, A., 1991. El Batolito de la Patagonia Central: evidencias de un magmatismo Triásico-Jurásico asociado a fallas transcurrentes. Rev. Geol. Chile 18 (2), 121–138.
Rhys, D.A., Lewis, P.D., Rowland, J.V., 2020. Structural controls on ore localization in epithermal gold-silver deposits: a mineral systems approch. Rev. Econ. Geol. 21, 83–145.
Riel, N., Jaillard, E., Martelat, J.-E., Guillot, S., Braun, J., 2018. Permian-Triassic Tethyan realm reorganization: implications for the outward Pangea margin. J. South Am. Earth Sci. 81, 78–86. https://doi.org/10.1016/j.jsames.2017.11.007.
Riley, P., Linker, J.A., Mikic, Z., 2001. An empirically-driven global MHD model of the solar corona and inner heliosphere. J. Geophys. Res. 106 https://doi.org/10.1029/2000JA000121.issn:0148-0227.
Rose, A.W., Hawkes, H.E., Webb, J.S., 1979. Geochemistry in Mineral Exploration. Academic Press, New York, p. 657.
Rowland, J.V., Simmons, S.F., 2012. Hydrologic, magmatic, and tectonic controls on hydrothermal flow, Taupo volcanic zone, New Zealand—implications for the formation of epithermal vein deposits. Econ. Geol. 107, 427–457.
Saxby, J.D., 1976. Significance of organic matter in ore genesis. In: En, Wolf, K.H. (Eds.), Handbook of Strata-Bound and Stratiform Ore Deposits 2. Elsevier, Amsterdam, pp. 112–133.
Schalamuk, I., De Barrio, R., Zubia, M., Genini, A., Hecheveste, H., 1999. Provincia Auroargentífera del Deseado, Santa Cruz. In: En Zapettini, E. (Ed.), Recursos Minerales de la República Argentina, vol. 35. Instituto de Geología y Recursos Minerales SEGEMAR, Anales, Buenos Aires, pp. 1177–1188.
Schneiderholm, H., 1923. Chalcographishe untersuchung des Mansfelder kupferschiefers: Neues Jahrbuch für Mineralogie. Geologie und Paleontologie 47, 1–38.
Seebeck, H., Nicol, A., Walsh, J.J., Childs, C., Beetham, R.D., Pettinga, J., 2014. Fluid flow in fault zones from an active rift. J. Struct. Geol. 62 https://doi.org/10.1016/j.jsg.2014.01.008.
Zerfass, Chemale Jr., F., Schultz, C.L., Lavina, E.L., 2004. Tectonics and sedimentation in Southern South America during Triassic. Sediment. Geol. 166, 265–292. https://doi.org/10.1016/j.jsames.2009.03.003.
Secretaría de política minera, 2020. Catastro Minero Unificado [online]. Available at http://cima.minem.gob.ar/dataset/2100/catastro-minero-unificado%3e%20 [revised February 21, 2020].
Sibson, R.H., 2000. Fluid involvement in normal faulting. J. Geodyn. 29 (3–5), 469–499. https://doi.org/10.1016/s0264-3707(99)00042-3.
Sibson, R.H., 1996. Structural permeability of fluid-driven fault-fracture meshes. J. Struct. Geol. 18, 1031–1042.
Simpson, G., 1933. Stratigraphic nomenclature of the early tertiary of central patagonia. Am. Mus. Novit. 644, 1–13.
Storey, B.C., Alabaster, T., Pankhurst, R.J., 1992. Magmatism and the causes of continental break-up. Geol. Soc. Lond. Spec. Publ. 68, 404.
Storey, B.C., Kyle, P.R., 1997. An active mantle mechanism forGondwana breakup. S. Afr. J. Geol. 100 (4), 283–290.
Storey, B.C., Vaughan, A.P.M., Riley, T.R., 2013. The links between large igneous provinces, continental break-up and environmental change: evidence reviewed from Antarctica. Earth Environ. Sci. Trans. Roy. Soc. Edinburgh 104, 1–14.
Tassara, S., González-Jiménez, J.M., Reich, M., Schilling, M.E., Morata, D., Begg, G., Corgne, A., 2017. Plume-subduction interaction forms large auriferous provinces. Nat. Commun. 8 (1) https://doi.org/10.1038/s41467-017-00821-z.
Tharalson, E.R., Monecke, T., Reynolds, T.J., Zeeck, L., Pfaff, K., Kelly, N.M., 2019. The distribution of precious metals in high-radebanded quartz veins from low-sulfidation epithermal deposits: Con-straints from μXRF mapping. Minerals 9.
Viera, R., Pezzuchi, H., 1976. Presencia de sedimentitas pérmicas en contacto con rocas del "Complejo metamórfico" de la Patagonia Extraandina, Ea. dos Hermanos, provincia de Santa Cruz. Revista Asoc. Geol. Argent. 31 (4), 281–283.
Vollgger, S.A., Cruden, A.R., Ailleres, L., Cowan, E.J., 2015. Regional dome evolution and its control on ore-grade distribution: insights from 3D implicit modelling of the Navachab gold deposit, Namibia. Ore Geol. Rev. 69, 268–284. https://doi.org/10.1016/j.oregeorev.2015.02.020.
Zambrano, J.J., Urien, V.M., 1970. Geological outline of the basins in Southern Argentina and their continuation off the Atlantic Shore. J. Geophys. Res. 75. No 8.